

UCLA

UCLA Electronic Theses and Dissertations

Title

Lysozyme-Triggered Nanodiamond Contact Lens for Glaucoma Treatment &
Phenotypically-based Combinatorial Drug Optimization for Multiple Myeloma Treatment

Permalink

<https://escholarship.org/uc/item/1mr8m6g5>

Author

Zhang, Kangyi

Publication Date

2015

Peer reviewed|Thesis/dissertation

UNIVERSITY OF CALIFORNIA

Los Angeles

Lysozyme-Triggered Nanodiamond Contact Lens for Glaucoma Treatment

&

Phenotypically-based Combinatorial Drug Optimization for Multiple Myeloma Treatment

A dissertation submitted in partial satisfaction of the
requirements for the degree Doctor of Philosophy

in Oral Biology

by

Kangyi Zhang

2015

ABSTRACT OF THE DISSERTATION

Lysozyme-Triggered Nanodiamond Contact Lens for Glaucoma Treatment

&

Phenotypically-based Combinatorial Drug Optimization for Multiple Myeloma Treatment

by

Kangyi Zhang

Doctor of Philosophy in Oral Biology

University of California, Los Angeles, 2015

Professor Dean Ho, Chair

In glaucoma treatment, ocular devices such as drug-loaded contact lenses have recently emerged as preferred candidates over eyedrops. Timolol maleate (TM), a prevalent glaucoma drug, exhibits side effects when excess drug enters the systemic circulation. Unlike eyedrops and drug-soaked lenses, new designs should provide sustained release and minimize undesirable burst release. Current innovations have not addressed the important issue of drug elution from contact lens during wet storage and shipment. Here we present a nanodiamond (ND)-embedded contact lens capable of lysozyme-triggered release of TM for sustained therapy. We found that ND-nanogel containing lysozyme-cleavable polymers enabled the controlled and sustained release of TM in the presence of lysozyme. Nanodiamonds also improved the mechanical properties of the poly-HEMA lenses without compromising on water content, oxygen permeability and optical clarity. In vitro cell viability assays on primary trabecular meshwork cells revealed that the released TM retained their antioxidant activity – an indicator of timolol efficacy.

This successful lysozyme activation of our functionalized ND nanogel can be easily applied to other diseases and drugs where localized triggered release is desired.

Conventional combinatorial treatment for multiple myeloma and other cancers uses an additive approach of maximum tolerated doses from single-drug experiments. These doses do not reflect true drug behavior in combinatorial therapy. A rapid and robust platform is necessary to optimize multiple parameters to find the best drug combination for improved efficacy and safety. Here, we present Response Surface Optimization (RSO) where we rapidly narrowed down our top three myeloma drug candidates (Bortezomib-Panobinostat-Dexamethasone) from a starting list of fourteen drugs in a short span of five months. The mechanism-independent RSO platform screens drugs based on maximizing the therapeutic window – increased healthy cell viability and decreased cancer cell viability. After the 1st iteration experiment, a linear regression experimental process (equation) is generated using MATLAB to reconcile the empirical data. Undesirable candidates are removed before performing a 2nd screening iteration. In the 3rd iteration, the optimum drug concentrations of the best drug combinations are determined. Response surface maps for output based on multi-parameters are plotted and the optimum is determined. Interestingly, this three-drug combination was the focus of recent myeloma clinical trials for refractory and relapsed patients. While conventional drug screening approaches demand huge time and money investment, the RSO platform rapidly and accurately converges on prime solutions. The RSO is applicable to the clinic where inter-patient variability requires adaptive treatment interventions based on individual clinical outcomes.

The dissertation of Kangyi Zhang is approved.

Daniel T. Kamei

Kang Ting

Wenyuan Shi

Dean Ho, Committee Chair

University of California, Los Angeles

2015

TABLE OF CONTENTS

Acknowledgements	ix
Biographical Sketch	x
Lysozyme-Triggered Nanodiamond Contact Lens for Glaucoma Treatment	1
- Background and Significance	2
- Methodology	5
- Results and Discussion	10
Phenotypically-based Combinatorial Drug Optimization for Multiple Myeloma Treatment	17
- Background and Significance	17
- Methodology	20
- Results and Discussion	23
Figures for “Lysozyme-Triggered Nanodiamond Contact Lens for Glaucoma Treatment” (Details on page vi)	34
Figures for “Phenotypically-based Combinatorial Drug Optimization for Multiple Myeloma Treatment” (Details on page vi)	43
Bibliography	58

LIST OF FIGURES

Figure A1: Schematic illustration of our lysozyme-activated drug eluting contact lens	35
Figure A2: Characterization of ND-nanogel during synthesis	36
Figure A3: FTIR spectra of chitosan and N-acetylated chitosan	37
Figure A4: Characterization of physical properties of contact lenses	38
Figure A5: SEM images of poly-HEMA lens and ND-nanogel lens	39
Figure A6: Enzyme-triggered drug release of ND-nanogel lens	40
Figure A7: Fluorescence spectral scan of Alexa Fluor® 488-labeled NDs in water and eluted solution from ND-nanogel lens	41
Figure A8: Evaluation of the antioxidant capacity of timolol using primary human trabecular meshwork cells	42
Figure B1: Flowchart of the three stages of the Response Surface Optimization (RSO)	44
Figure B2: Schematic showing the background of the multiple myeloma collaboration between National University of Singapore and University of California, Los Angeles	45
Figure B3: An excerpt of the list of drug combinations in the second iteration	46

Figure B4: Table showing the design of the three iterations	47
Figure B5: List of 14 drugs used for the 1 st iteration	48
Figure B6: MATLAB multi-drug optimization experimental assessment of first iteration (first attempt)	49
Figure B7: MATLAB multi-drug optimization experimental assessment of first iteration (second attempt)	50
Figure B8: Multi-drug optimization experimental assessment for the 2 nd iteration with 9 drug candidates	51
Figure B9: Multi-drug optimization experimental assessment for the 3 rd iteration with 5 drug candidates	52
Figure B10: Four diagnostic plots generated specifically for the third iteration	53
Figure B11: Excerpt of the top 20 prescribed combinations in a multi-drug optimization experimental assessment.	54
Figure B12: Excerpt of the top 10 and bottom 10 prescribed combinations consisting of two or three drugs.	55

Figure B13: Pearson correlation plots for prescribed outputs vs experimental outputs.	56
Figure B14: Examples of experimentally-derived response surface plots for the second iteration with nine drugs.	57

ACKNOWLEDGEMENTS

This thesis contains a version of a published journal article in ACS Nano.

Ho Joong Kim, Kangyi Zhang, Laura Moore, and Dean Ho, “Diamond Nanogel-Embedded Contact Lenses Mediate Lysozyme-Dependent Therapeutic Release.” *ACS Nano* 8, no. 3 (2014): 2998–3005. doi:10.1021/nn5002968

Ho Joong Kim and Kangyi Zhang are co-authors. HJ Kim conceived of the design of the nanodiamond contact lenses and all chemical synthesis. Both HJ Kim and K Zhang evaluated the properties of the ND-nanogel and contact lenses. Both authors did the drug elution study. K Zhang performed the biological assays to check for drug efficacy.

Research is made possible thanks to the National Science Foundation CAREER Award (CMMI-0846323), Center for Scalable and Integrated Nano-Manufacturing (DMI-0327077), CMMI-0856492, DMR-1105060, V Foundation for Cancer Research Scholars Award, Wallace H. Coulter Foundation Translational Research Award, Society for Laboratory Automation and Screening (SLAS) Endowed Fellowship, Beckman Coulter, and National Cancer Institute Grant U54CA151880.

K. Zhang gratefully acknowledges individual fellowship support provided by Agency for Science, Technology and Research (A*STAR). K Zhang would like to thank Prof. Ho, Prof. Ting, Prof. Kamei, Prof. Shi, his parents and fellow laboratory members for their support throughout his PhD.

BIOGRAPHICAL SKETCH

2009 - Brown University, BS, Biomedical Engineering

2012 - Northwestern University, MS, Biomedical Engineering

Kangyi Zhang is a recipient of the Agency for Science, Technology and Research (A*STAR) BS-PhD scholarships. He is a member of the following honorary societies: Tau Beta Pi, Sigma Xi, Phi Beta Kappa and American Chemistry Society.

Publications

Ni M, Teo JC, Ibrahim MS, Zhang K, Tasnim F, Chow PY, Zink D, Ying JY, Characterization of membrane materials and membrane coatings for bioreactor units of bioartificial kidneys, *Biomaterials*. **2011** Feb;32(6):1465-76

Man HB, Zhang K, Robinson E, Chow EK, Ho D, Engineering Nanoparticulate Diamond for Applications in Nanomedicine and Biology, *Chapter 15 Ultrananocrystalline Diamond 2nd Edition* **2012** Shenderova, Elsevier

Kim HJ, Zhang K, Moore L, Ho D, Diamond Nanogel-Embedded Contact Lenses Mediate Lysozyme-Dependent Therapeutic Release, *ACS Nano* **2014** 8 (3) ; 2998–3005

Wang H, Lee DK, Chen KY, Chen JY, Zhang K, Silva A, Ho CM, Ho D, Mechanism-Independent Optimization of Combinatorial Nanodiamond and Unmodified Drug Delivery Using a Phenotypically-Driven Platform Technology, *ACS Nano* **2015** 9 (3) ; 3332-3344D

Conferences

Zhang K, Kim HJ, Gatica M, Moore L, Chow EK, Ho D, Nanodiamond Therapeutic Delivery Vehicles for Cancer Treatment and Regenerative Medicine, *International Association for Dental Research* (20-23th Mar 2013) Seattle WA

Zhang K, Kim HJ, Daneshgaran G, Yen A, Ho D, Nanodiamond-embedded chitosan hydrogel for localized, sustained, and targeted delivery of celecoxib against oral cancer, *Materials Research Society* (21-25th April 2014), San Francisco, CA

Cao YP, Kaplan A, Zhang K, Fei F, Youn LY, Lux R, Ho D, Kang M, *In Vitro* Effect of Nanodiamond on Oral Bacterial Biofilm, *American Association of Endodontists* (30th April-3rd May 2014) Washington DC

Zhang K, Kim HJ, Moore L, Ho D, Nanodiamond Gel-Embedded Polymer Matrices for Triggered Therapeutic Release, *International Association for Dental Research* (25-28 June 2014) Cape Town, South Africa

Patents

Kim HJ, Zhang K, Ho D, Diamond Nanogel-Embedded Contact Lens for Lysozyme Triggered Glaucoma Therapy, *Northwestern University, NU2014-005*

Zhang K, Silva A, Ho C-M, Ho D, Novel Optimized Drug Combinations for Drug-Resistant and Drug-Sensitive Multiple Myeloma Developed using a Systematic Phenotypic Personalized Medicine Platform, *University of California, Los Angeles, Case No. 2015-795*

Lysozyme-Triggered Nanodiamond Contact Lens for Glaucoma Treatment

published¹ in

Ho Joong Kim, Kangyi Zhang, Laura Moore, and Dean Ho

“Diamond Nanogel-Embedded Contact Lenses Mediate Lysozyme-Dependent Therapeutic Release.”

ACS Nano 8, no. 3 (2014): 2998–3005. doi:10.1021/nn5002968

(This journal article is an open access article under an ACS AuthorChoice License, which permits copying and redistribution of the article or any adaptations for non-commercial purposes.)

BACKGROUND & SIGNIFICANCE

By the year 2020, glaucoma would affect approximately 79.6 million people, of which a larger proportion would consist of Asians and women². Glaucoma occurs when the optic nerve is damaged due to excessive intraocular pressure from abnormal drainage of aqueous humor. The application of therapeutic eyedrops is the traditional treatment method but the necessity for frequent applications has led to poor patient compliance³⁻⁵ and safety concerns.

Eyedrop administration results in short bursts of high drug concentrations locally. Besides drug wastage from fluid outflow, such concentration levels are typically above the therapeutic window and this leads to adverse localized and systemic effects. The widely used glaucoma drug timolol maleate (TM) is a beta-blocker which can cause adverse cardiovascular and pulmonary side effects^{6,7}. Devices which allow extended drug release means fewer drug application, increased patient compliance, increased efficacy and lowered toxicity. These devices include drug-loaded PLGA films⁸, drug-hydrogel fornix inserts⁹, therapeutic contact lenses and microelectromechanical systems (MEMS)¹⁰. Recent innovations in therapeutic contact lenses include the use of microparticles, films and molecularly imprinted hydrogels¹¹⁻¹⁶. Unlike eyedrops and drug-soaked lenses, which show burst release profiles, novel contact lenses made through molecular imprinting or embedded microparticles maintain a local therapeutic dosage for a longer time.

For any drug delivery system to be clinically translatable and commercially viable it must not only be effective, but also be readily manufactured and distributed. One of the manufacturing and distribution challenge with soft contact lenses is that they are typically made of poly-2-hydroxyethyl methacrylate (polyHEMA), which becomes brittle when dry. Therefore, most soft

contact lenses are distributed in wet storage using a small amount of water or buffer. However, when drug-loaded contact lenses are in wet storage, the drug will elute into the solution prematurely, rendering the drug delivery system ineffective. This has necessitated the development of smarter delivery systems, which release their therapeutic payload under artificial or biological stimuli¹⁷. One potential biological stimulus is lysozyme, an enzyme naturally present in lacrimal fluid that catalyzes the hydrolysis of β -1,4-glycosidic bonds present in peptidoglycans and chitodextrins. Here, we propose an enzyme-triggered delivery system, where the drug is sequestered within the contact lens until it is released by lysozyme-mediated cleavage upon eye application.

Recently, nano-materials have been producing exciting results in the field of biomedical imaging and drug delivery¹⁸⁻²⁰. In particular, nanoparticles have been remarkably effective vehicles for ocular delivery of bioactive molecules, such as small molecule therapeutics and nucleic acids²¹. One especially promising nanoparticle is the nanodiamond (ND), which has a uniquely faceted carbon surface²² that has been harnessed for a variety of purposes in biomedical imaging, sensing and therapeutic delivery²³⁻²⁵. In addition to being highly effective nano-carriers, NDs have been found to be highly biocompatible in a variety of *in vitro* and *in vivo* studies²⁶⁻²⁸. Comparing controls and mice treated with high doses of NDs or NDs carrying chemotherapeutics, there is no significant difference in hematological or serum markers of inflammation and toxicity²⁷. Additionally, histological analysis of the kidney, liver and spleen found no difference between NDs and PBS controls²⁹. Although the ocular compatibility of NDs has not yet been tested, carbon nanohorns, a related and similarly sized material, do not induce any clinical abnormalities on eye irritation tests in rabbits³⁰.

Here we present the design, synthesis and characterization of an ND-embedded contact lens capable of controlled release of timolol maleate (TM). Nanodiamonds have previously been incorporated into polymer matrices in order to improve the mechanical properties and/or elute therapeutic molecules^{23,31,32}. In addition, previous reports have demonstrated the ability to produce and utilize optically transparent ND films³³ - a critical design consideration for a diamond-based contact lens. All these information support the development of an ND-based contact lens for controlled delivery of glaucoma therapeutics. For this work, individual NDs are first coated in highly branched polyethyleneimine (PEI) and then cross-linked with the enzyme-cleavable polysaccharide, chitosan, to form an ND-nanogel encapsulating TM [Fig. A1 a]. The drug-loaded ND-nanogels are then embedded within a polyHEMA matrix and cast into contact lenses, which can elute timolol in the presence of lysozyme [Fig. A1 b].

METHODOLOGY

Preparation and Characterization of Timolol-loaded ND-Nanogel

ND-nanogels are made by cross-linking ND-PEI (polyethylenimine) clusters with N-acetylated chitosan to form a lysozyme degradable nanogel [Fig A1 a]. The NDs must be well dispersed in our hydrogel matrix in order to maintain optical clarity. Electrostatic and covalent interactions, mediated by surface graphitic carbon, cause primary diamond particles (~5 nm) to spontaneously form clusters of up to 200 nm. To remove the graphitic carbon, freeze-dried pristine NDs were air oxidized at 420°C for 2.5 hrs. This oxidation also improves the homogeneity of the surface chemical groups, converting them into carboxylic acids and cyclic acid anhydrides³⁴. The NDs were then dissolved in anhydrous DMSO and ultrasonicated for 30 min.

The covalent conjugation of highly-branched PEI increases the number of surface reactive sites for cross-linking. In addition, PEI spaces out the NDs in the nanogel and allows better lysozyme penetration. After PEI attachment, the amine (-NH₂) groups are converted into carboxylic acid (-COOH) groups. To the oxidized NDs in DMSO, 1-ethyl-3-(3-dimethylaminopropyl) carbodiimide (EDC) and N-hydroxysuccinimide (NHS) were added. After stirring for 1 hr, excess PEI800 was added to the solution and stirred overnight. The product was washed with water in consecutive washing/centrifugation cycles. ND-PEIs were conjugated with excess succinic acid to yield carboxylated ND-PEIs.

Chitosan is a linear polysaccharide composed of D-glucosamine and N-acetyl-D-glucosamine coupled with 1,4-β-glycosidic bonds that can be cleaved by lysozyme. The rate at which

chitosan is degraded by lysozyme is dependent on the degree of acetylation (DA), with increased acetylation associated with more rapid degradation³⁵. Prior to coupling to ND-PEI, chitosan is acetylated to 50% DA (degree of acetylation) using acetic acid according to the protocol by Ren et al³⁵.

Chitosan was first dissolved in 3 % (v/v) acetic acid solution before the addition of MeOH (methanol). Acetic anhydride was added to the solution, stirred at room temperature overnight and then neutralized with 1 mol/L NaOH to yield a white precipitate. The collected precipitate was washed with water in wash/centrifugation cycles and lyophilized to give a white powder. The degree of N-acetylation (DA) of chitosan was calculated from elemental analysis.

Amide cross-linking reaction was performed between N-acetylated chitosan and NHS-activated ND-PEI in the presence of timolol, yielding timolol-loaded ND-nanogel [Fig A1 a]. All functionalized NDs were confirmed by FTIR (Nexus 870 spectrometer (Thermo Nicolet)). TEM images were taken using a 200kV JEOL JEM-2100F TEM. Hydrodynamic size and ζ -potential measurements were performed using Zetasizer Nano ZS (Malvern Instruments, Malvern, UK) using NDs in deionized water at 50 μ g/ml.

Preparation of ND-Embedded Contact Lenses

The contact lenses were prepared by free-radical copolymerization. ND-nanogels were suspended in HEMA solution before the addition of MAA (5% v/v), ethylene glycol dimethacrylate (EGDMA) (0.25% v/v) and Darocur (photoinitiator, 0.2 % v/v). This composition was chosen because it is commonly used to make soft contact lenses with an average pore size of 34.7 \AA ³⁶. This would be suitable for the penetration of lysozyme (30x30x45 \AA). The monomer

solution was poured into an aluminum mold with 0.50 mm center thickness. Polymerization was initiated with UV irradiation (6.5 mW/cm² at 365 nm). The gel was soaked in deionized water for 4 hrs and discs (12 mm diameter) were punched out with a cork borer. The lenses were then immersed in 0.9% NaCl solution for 2 days to remove unreacted monomers and initiator. For comparisons, molecularly imprinted contact lenses and drug-soaked lenses were manufactured as previously described¹⁴. Drug loading was done by soaking in 0.02 mM of timolol solution for 3 days.

Characterization of Contact Lenses

Besides enabling lysozyme-triggered drug release, our ND-nanogel contact lenses must match the acceptable ranges of various properties of commercial lenses. Water content, mechanical strength and optical transparency are important parameters for evaluation.

SEM images were obtained using a Hitachi S-4800-II. Samples were lyophilized before being coated twice with 5 nm thick OsO₄ using an osmium plasma coater (Structure Probe, Inc.). Rectangular specimens were placed on Instron 5533 and tested with three 10% length preload cycle stretches before an ultimate strength test. The modulus of elasticity of each lens was calculated by using the initial 5% slope from the stress-strain graph. The water content of contact lenses was calculated by the ratio of the weight of water in the hydrogel to the total weight of the hydrogel.

Determining Timolol-Release Profiles

The novelty of this research lies in the lysozyme-triggered release of timolol drug from our contact lens. The release profile of our ND-nanogel lenses has to be compared with that of controls – drug-soaked and molecularly imprinted lenses.

The release of timolol at 37.8 °C from hydrogels was measured in triplicate over 72 hrs in 5mL of saline or artificial lacrimal fluid (6.78 g/L NaCl, 2.18 g/L NaHCO₃, 1.38 g/L KCl, 0.084 g/L CaCl₂, pH 7.2). Timolol-release profile was carried out using a Varian high performance liquid chromatography (HPLC) (Milford, MA,USA). A mixture of 0.1M PBS at pH 2.8 : methanol (40:60) delivered at 1.0 ml/min was used as the mobile phase. The peak area at 295 nm was used for calculation.

Culturing of Human Trabecular Meshwork (HTM) Cells

The timolol must retain its drug efficacy after eluting out of the ND-nanogel contact lenses. We tested this using human trabecular meshwork cells which are located near the ciliary bodies of the eye. These cells are responsible for proper drainage of aqueous humor. Timolol would protect these trabecular meshwork cells against oxidative stress induced by hydrogen peroxide. Higher cell viability is expected with this timolol pre-treatment and we test this using two cell viability assays – XTT and CellTiter-Blue.

Primary HTM cells (P10879, Innoprot) were propagated in fibroblast growth medium-2 (CC-3132 Lonza) with the provided supplement kit and 1% (v/v) penicillin-streptomycin. Cells were maintained in a humidified incubator (37°C, 5% CO₂). At 80% confluence, the cells were

trypsinized for subculturing or for experiment. After four days of lysozyme addition to the gel, the eluate, which contained timolol, was used for the experiments.

Determination of Cell Viability via XTT Assay

The eluate was diluted to a timolol concentration of 1 µg/ml before being applied to the HTM cells (P5) for 10 min. Hydrogen peroxide (0.2µM) was then applied for 15 min. The XTT media was prepared by adding 1.5ml of XTT (Invitrogen) solution (1 mg/ml XTT in PBS) and 6.46µl menadione (Enzo Life Sciences, 10 mg/ml ethanol) to 8.5 ml of media. For the assay, 50µl of XTT media was added to 100µl of fresh media in each well. PBS washing was done once in between these steps. The plate was incubated for 2 hrs at 37°C, shaken and read at 450nm with a spectrophotometer. Cell viability was expressed as a ratio to the control wells.

Determination of Cell Viability via CellTiter-Blue Assay

The eluate was diluted to a timolol concentration of 1 µg/ml before being applied to the HTM cells for 10 min. Hydrogen peroxide (20µM) was then applied for 30 min. 20 µl CellTiter-Blue (Promega) was then added to each well containing 100µl of media. The plate was incubated for 2 hrs at 37°C and read at 560nm/590nm (emission/excitation). Higher fluorescence readings indicate higher viability.

RESULTS AND DISCUSSION

ND-Nanogel Synthesis and Characterization

For optimal contact lens fabrication and to ensure clinical-grade optical clarity, the NDs must be well dispersed in the poly-HEMA hydrogel matrix. One main cause of spontaneous agglomeration of NDs is the presence of surface graphitic carbon, which can be eliminated by air oxidation³⁷. This oxidation method also improves the homogeneity of the surface chemical groups, converting the majority into carboxylic acids and cyclic acid anhydrides³⁸. Fourier Transform Infrared (FTIR) spectra of the furnace-treated NDs shows the addition of a carboxylic acid C=O stretching peak at 1775 cm^{-1} , indicating successful oxidation [Fig. A2 a]. In addition, ζ -potential measurements show a shift from an average of +36.8mV for the pristine NDs to -40.7mV for the air oxidized NDs, confirming the addition of carboxylic acid [Fig. A2 b]. The air oxidized NDs, which form a stable colloidal solution, have an average particle size of 32.2 nm [Fig A2 b].

To increase the surface density and accessibility of reactive groups, the oxidized NDs are then coated with highly branched PEI-800 using 1-Ethyl-3-(3-dimethylaminopropyl)carbodiimide (EDC) and N-Hydroxysuccinimide (NHS). FTIR analysis of ND-PEI is indicative of amide bond formation between ND-surface carboxylic acids and primary amines on PEI, showing peaks at 3380, 2950 and 2825 1640 and 1560 cm^{-1} [Fig. A2 a]. Compared to oxidized NDs, ND-PEI show a slight increase in size ($\sim 6\text{ nm}$) and a change in the average ζ -potential to +39.4 mV. This is consistent with the addition of positively charged amine groups from PEI to the particle surface [Fig. A2 b]. Comparison of the TEM images of pristine NDs and ND-PEI shows that ND-PEI particles are larger, smoother and more electron-dense than the pristine particles [Figs. A 2c, d].

This work presents a novel method for dispersion and stabilization of reactive NDs in water, facilitating the biological or chemical functionalization of NDs without the use of organic solvents.

The synthesis of the ND-nanogels was achieved by crosslinking ND-PEI clusters with N-acetyl chitosan to form a lysozyme-degradable nanogel. Chitosan was acetylated to 50% DA (elemental analysis) using acetic acid according to the protocol used by Ren et al³⁵ prior to coupling to ND-PEI. The confirmation of acetylation was verified with FTIR [Fig. A3]. ND-PEI was first modified with succinic anhydride and then coupled to acetylated chitosan using EDC/NHS in the presence of timolol [Fig. A1 a]. This procedure generates the drug-encapsulated, enzyme-cleavable ND-nanogels, which can then be embedded in a contact lens.

FTIR analysis of the ND-nanogel demonstrates the characteristic peaks for amide bonds and primary amines, which is consistent with the presence of chitosan and PEI [Fig. A2 a]. Although NDs conjugated PEI and chitosan cannot be distinguished on FTIR, entrapment of drug is confirmed by the presence of characteristic peaks for TM at 2967, 2853, 1705, and 1375 cm^{-1} [Fig. A2 a]. In addition, DLS data shows that the ND-nanogels have an average diameter of 120nm [Fig. A2 b] which is much larger than ND-PEI. TEM images also show each nanogel as a network of individual NDs [Fig. A2 e]. Finally, the average ζ -potential for the ND-nanogels is +38.2 mV, which is consistent with the presence of positively charged surface groups, such as the amines on PEI and/or chitosan [Fig. A2 b].

Contact Lens Synthesis and Characterization

In order to serve as an effective ocular drug delivery platform the ND-nanogels were then incorporated into a poly-HEMA matrix and cast into contact lenses. In addition to porosity, the optical clarity and water content of poly-HEMA gels make them ideal for soft contact lenses. The addition of the ND-nanogels to the poly-HEMA lens does not induce any notable alterations in the lens optical characteristics [Fig. A4 b,c]. Optical clarity was quantified by average percent light transmission across the visual spectrum (400-700nm). The poly-HEMA contact lens shows an average transmission of 93.8% without ND-nanogel loading, 87.4% with 0.1% ND-nanogel (w/w) and 84.5% with 0.2% ND-nanogel (w/w) [Fig A4 c].

Another important parameter in the design of therapeutic contact lenses is the water content. Water content dictates the oxygen permeability of the lens in addition to affecting lysozyme penetration and drug elution. The addition of the ND-nanogels, pristine NDs or PEI-Chitosan has little impact on the overall water content, with values ranging from 63.3% to 64.5% [Fig. A4 c]. Additionally, analysis of the contact lens surface by scanning electron microscopy (SEM) showed that the surfaces poly-HEMA and ND-nanogel embedded lenses are similar [Fig. A5]. The only observable difference is the presence of approximately 100nm ND-nanogels on the ND-nanogel lens surface. Given that the additives comprise only 0.1% (w/w) of the total lens mass, it is expected that the bulk characteristics of the gel would not be altered markedly.

As the contact lenses are subjected to innumerable mechanical stresses during the course of insertion, use and removal, the mechanical properties of the lens matrix are important. Previous reports on polymer matrices with embedded NDs have demonstrated enhancement in mechanical properties with the addition of a small amount of diamond²³. Tensile strength testing

of the contact lenses demonstrates that the addition of drug-loaded ND-nanogels (0.1% and 0.2% w/w) to the poly-HEMA lens boosts the Young's modulus to approximately 0.2MPa. This is an improvement of 40-50% from the unaltered lens [Figs. A4 d,e]. Similarly, the addition of pristine NDs (0.1% w/w) to the lens improves the Young's modulus by 31%. In contrast, the control lenses containing PEI-Chitosan (0.1% w/w) showed no alterations in mechanical properties. Combined these results indicate that incorporation of the ND particles into the contact lens reinforces the polymer matrix. For comparison, the ND-embedded hydrogels (at 0.2 MPa) are still far less stiff than conventional hard contact lenses, which boast a modulus of approximately 0.5 MPa. The lack of professional lens fabrication equipment may explain this discrepancy. Nevertheless, NDs make an attractive lens nanofiller due to their ability to improve tensile strength without altering overall lens thickness. Soft contact lens design is a balancing act between lens mechanical strength and oxygen diffusion, thicker lenses being stronger but they limit the amount of oxygen that reaches the cornea. NDs could make an attractive lens nanofiller due to their ability to improve tensile strength without increasing lens thickness.

Lysozyme-Triggered Delivery of Timolol Maleate

Although ND-nanogels improve the mechanical properties of the lenses, the goal of these studies is to produce contact lenses capable of releasing timolol in a controlled manner. The elution of TM was studied using high-performance liquid chromatography (HPLC) in 3 different types of contact lenses: ND-nanogel lens, drug-soaked lens and molecularly imprinted lens¹⁴. Drug release was studied in artificial lacrimal fluid or saline solution at pH 7.4, 37°C and with 2.7 mg/mL lysozyme. Both the drug soaked and molecularly imprinted contact lenses show nearly complete release of the TM within the first two hours [Fig. A6]. In contrast, in the absence of lysozyme, TM release from the ND-nanogel lens is undetectable. After treatment with lysozyme

the ND-nanogel released 9.41 μ g of TM in an approximately linear manner over 24 hours [Fig. A6]. Some variability in the TM release profile, including some burst release in one replicate, was observed after 48 hours of lysozyme treatment. This is likely due to variation in the size and depth of ND-nanogels within the polymer matrix and could likely be eliminated with minimal optimization and the utilization of commercial-grade lens fabrication equipment. However, the behavior after 48 h is less concerning because the lenses are meant for 24 hours usage. Additionally, TM release was not associated with ND release from the lens, as determined by tracking fluorescently labeled ND-PEI [Fig. A7]. Although NDs have previously been shown to be highly biocompatible, the stable retention of NDs is an additional safety assurance to users.

For the ND-nanogel lens to find clinical utility, it must be able to elute a sufficient amount of drug over 24 h. The recommended starting dosage of TM is two drops of 0.25% solution per day. Assuming a typical eye drop volume of 25 μ L and bioavailability of 1%, the total dosage would be 1.7 μ g/day⁹. Because the thickness of the lenses generated here is seven times as thick as a standard contact lens (700 μ m vs 100 μ m), the amount of drug released must be scaled. Taking the fractional mass released as inversely proportional to the square of the lens thickness, the commercial version of the ND-nanogel lens will release about 0.192 μ g/day or 11.3% of the standard dosage. However, a recent pharmacodynamics study using dogs showed that drug-soaked lenses releasing 20% of the standard eye drop dosage are capable of achieving the same efficacy as the eye drops³⁹. Hence, further optimization of the ND-nanogel lens would yield a clinically relevant and commercially viable product.

Biological Activity of Released Drug

In order to produce a clinically relevant entity, the TM released from the lens must retain its functionality. Confirmation of the biological activity of TM after elution from the contact lens was determined based on the drug's antioxidant capacity⁴⁰. Human trabecular meshwork cells were treated with TM prior to incubation with hydrogen peroxide to induce oxidative damage and lower cell viability. Cell viability was assessed using two separate assays – absorbance-based XTT, which measures mitochondrial enzyme activity, and fluorescence-based CellTiter-Blue™, which measures mitochondrial, cytoplasmic and microsomal enzyme activity. Cells pre-treated with standard or eluted TM prior to the addition of hydrogen peroxide show improved viability using both the XTT [Fig A8 a, $p < 0.005$] and CellTiter-Blue [Fig A8 b, $p < 0.0005$]. Importantly, there is no difference in cell viability between the standard and lens-eluted TM.

Conclusion

Overall, these studies have demonstrated that the ND-nanogel embedded contact lens provides an effective vehicle for the enzyme-triggered delivery of TM. The ND-PEI-chitosan nanogel provides a mechanism for TM sequestration prior to lysozyme activation while also improving the gel's mechanical properties. By sequestering the TM within the contact lens until its application on the eye, such contact lens eliminates the burst release observed with other lens types upon contact with water. This facilitates large-scale manufacturing and distribution of the therapeutic lenses. In addition, this work has provided a novel method for generating a stable, aqueous colloid of reactive NDs through the addition of PEI. ND-PEI provides a novel modification of the ND-platform that can be readily functionalized using aqueous chemistry. This is ideal for reactions where organic solvents cannot be used.

The system developed here based on NDs provides a novel platform for the development of hydrogels capable of enzyme-triggered drug release. The objective of the system was to provide glaucoma treatment via lysozyme-triggered release of timolol from a contact lens. However, because loading is achieved by drug encapsulation, virtually any therapeutic can be incorporated into the system for lysozyme-triggered delivery for the eye and other regions. Furthermore, the same approach could be applied to any number of biological systems by replacing chitosan with a different enzyme-cleavable polysaccharide. This type of nanoparticle-embedded hydrogel allows for enzyme-triggered drug release without the need for chemical modification of the therapeutic entity and without loss of structural integrity of the lens over time. By utilizing NDs in this novel approach to enzyme-triggered drug delivery, we are able to achieve superior mechanical performance in addition to effective drug delivery.

Phenotypically-based Combinatorial Drug Optimization for Multiple Myeloma Treatment

BACKGROUND & SIGNIFICANCE

Combinatorial Chemotherapy for Multiple Myeloma

Multiple myeloma is a malignant monoclonal plasma cell disorder characterized by infection, anemia, abnormal calcium and creatine blood concentrations, skeletal abnormalities, and renal failure^{41,42}. Approximately 0.7 percent of the population will be diagnosed with myeloma at some point in their lives and 3.3 per 100,000 adults will die every year⁴³.

Current combination drug therapy studies in myeloma clinical trials have shown much promise^{44,45}. Diseases, including cancer, involve numerous interactions between multiple molecular elements in a complex biological network⁴⁶. Multi-pronged disruption of cancer cell machinery, using drugs with complementary mechanisms, has resulted in improvements to progression-free survival and overall survival of patients^{42,47,48}. Compared to single-drug therapy, rationally-designed combinatorial treatments reduces systemic toxicity, accounts for tumor heterogeneity, and overcomes drug resistance^{47,49}.

Challenge of Combinatorial Chemotherapy – Determining Optimal Effective Dosages

Besides identifying the right drug combination, the major challenge to combinatorial therapy is determining the individual drug concentrations or drug dose ratio. Current additive design often uses the maximum tolerated dosages, determined in single drug treatment regime, for the

multiple-drug treatment regimes^{44,45}. However, such concentration levels are often higher than necessary and recent research is advocating the use of optimal effective dosages⁴². Reduced side effects and better drug efficacy can be achieved.

With the huge array of FDA-approved drugs for multiple-myeloma⁵⁰ and the need to determine the optimal effective dosages of each drug in combination therapy, a rapid and effective optimization platform is necessary. We have developed systemically designed and empirically-backed optimal drug combinations using a mechanism-independent optimization platform – Response Surface Optimization (RSO). We achieved this in five months while conventional drug discovery which produces non-optimal combinations based on additive design can take up to one decade. The output experimental information is solely based on cell viabilities of healthy control cells and cancer cells. This approach eliminates any uncertainty based on predictions of enzymatic network topology⁵¹. The goal is to maximize cancer cell death while minimizing patient toxicity. The mechanism-independent nature of the optimization platform employed here will markedly improve the de-risking of drug development and definitively pinpoint the most effective drug combinations optimized for multiple parameters simultaneously. RSO also allows personalized real-time adaptive drug combination selection – an important goal in modern clinical trials⁴⁷. Inter-patient tumor heterogeneity and evolved adaptive resistance mechanisms can be overcome using the RSO, which allows rapid prediction and tailoring of treatment regime to a particular patient. The patient's conditions serve as input data for RSO to rapidly fine-tune the combinatorial treatment regime in subsequent iterations.

Recently, our laboratory applied this mechanism-independent RSO platform to *in vitro* breast cancer studies⁵². Three breast cancer cell lines and three healthy cell lines were used. The drug candidates included nanodiamond-modified (doxorubicin, bleomycin, mitoxantrone) and -

unmodified drugs (paclitaxel). The list of drug combinations employed was generated using Latin hypercube sampling. The goal was to maximize the therapeutic window, which is calculated using the viability of healthy cells minus the viability of cancer cells. The collected experimental data are reconciled by regression analysis and the response surfaces of cellular viabilities can be plotted for various drug combinations. Using differential evolution algorithm, we rapidly converged on the global optimum of the response surface. These optimized combinations were once again applied to the various cell lines and experimentally verified. Based on therapeutic windows, optimized nanodiamond (ND) combinations outperformed randomly sampled ND combinations. Optimized ND-modified combinations outperformed optimized unmodified combinations, thus demonstrating the advantageous property of nanodiamonds.

METHODOLOGY

Response Surface Optimization (RSO) Platform & Drug Candidate Selection

This Response Surface Optimization (RSO) platform consists of three major stages: Design of drug combinations, *in vitro* cellular assay, and data analysis and optimization [Fig B1]. We began with fourteen drugs and conducted two iterations (experimental runs) to screen out unfavorable drug candidates. We then conducted a third iteration using five favorable drug candidates to determine the right drug concentrations. A listing of these fourteen drugs and the drugs which were screened out in each iteration is shown in Fig. B5. These fourteen drugs have been selected by our collaborator Prof. Edward Chow at the National University of Singapore. Four favorable drugs were selected from a pool of 114 drugs [Fig. B2]. The criterion is that the drug kills the resistant cell line (RPMI 8226p100v) more effectively than the sensitive line (RPMI 8226). The four chosen candidates are combined with ten FDA-approved drugs to make the drug candidates for our first iteration.

Orthogonal Array Composite Design (OACD)

In each iteration (experiment run), the list of drug combinations used is based on a research paper published by our collaborators at UCLA⁵³. The Orthogonal Array Composite Design (OACD) aims to reduce the number of required experiments to obtain sufficient information to build a mathematical equation. This OACD allows resolution IV designs at the 2-dosage level drug screening experiments – an advantage over Central Composite Design (CCD) and Small Composite Design (SCD)⁵³. At resolution IV, the main effects are not confounded with the interaction effect. This means we can retain or eliminate drug candidates in the initial screening

stages. An excerpt of the 2nd iteration is shown in Fig. B3. Details of the design of the three iterations are presented in a table format in Fig. B4.

In vitro Cellular Assay and the Desired Output

After the list of drug combinations is determined, they are applied to an *in vitro* cellular assay. A healthy control cell line (THLE-2) is used to determine liver toxicity caused by drug treatment. Drug efficacy is determined using the B lymphocyte cancer cell (RPMI 8226). Favorable drug combinations would maximize cancer cell killing while minimizing healthy cell death. Hence, our goal here is to maximize the output, which is the cell viability of THLE-2 minus the that of RPMI 8226. The experiments are conducted in a rapid, high throughput manner using an automated liquid handler machine.

Linear Regression Experimental Process

The outputs of these drug combinations are run through the programming software MATLAB to provide a linear regression experimental process to reconcile the actual experimental results. The function used is stepwise linear regression `{LinearModel.stepwise}`. Basically, stepwise regression adds or removes terms depending on their t-statistics of the respective coefficients. The resulting equation consists of terms which MATLAB considers to be significant. Only terms up to the power of 2 are considered because higher order terms are much smaller than first- and second- order terms⁵².

While each conducted experiment involves fewer than 200 drug combinations, the generated equation can prescribe the output of many more drug combinations and drug concentrations.

Once again, a key advantage of this RSO platform is that the optimal drug combinations are empirically-backed and not based on prediction. A linear regression experimental process (mathematical equation) is shown below.

$$y = \beta_0 + \beta_1 X_1 + \dots + \beta_n X_n + \beta_{1,2} X_1 X_2 + \dots + \beta_{m,n} X_m X_n + \beta_{11} X_1^2 + \dots + \beta_{nn} X_n^2$$

β refers to coefficients (numbers) while X_1 refers to the concentration of drug one etc. Similarly, $\beta_{1,2}$ refers to the coefficient of the two-drug term for $X_1 X_2$ (interaction of drug 1 and drug 2). The third set of terms refers to the squared terms of the single drugs - $\beta_{nn} X_n^2$.

MATLAB also provides the R^2 and adjusted R^2 values which explains the percentage accuracy of the mathematical equation. An adjusted R^2 value of 0.90 means 90% of the experimental data can be accounted for by the equation. The fitting correlation term is the square root of this R^2 . Diagnostic plots are also generated to affirm the validity of the data fitting. These plots are, "Plot of Residuals vs Fitted Values", "Case Order Plot of Cook's Distance", "Normality Probability Plot of Residuals" and "Histogram of Residuals".

RESULTS AND DISCUSSION

1st iteration (1st attempt) with 14 Drug Candidates

In the 1st and 2nd iterations, the process of selecting and eliminating drug candidates involves examining the experimental coefficients at the single and two-drug level. Since the output is the viability of control cells (THLE2) minus cancer cells (RPMI8226), we are aiming to maximize the output. Observing the single-drug level, undesirable drug candidates have negative coefficients and/or non-significant p values (>0.05). D1, D2, D5, D10 and D12 (Thalidomide, Lenalidomide, AMD3100, Actinomycin, Doxorubicin) are thus eliminated [Fig. B6]. Desirable drug candidates have positive coefficients and are significant at the 5% level. They are D4, D6, D7, D11, D13 and D14 (Zoledronic Acid, Bortezomib, Carfilzomib, Mitomycin C, Panobinostat, Dexamethasone). D3, D8, D9 (Cyclophosphamide monohydrate, Mechlorethamine HCl, Decitabine) are inconclusive. Examining two drug terms, we can eliminate D3 and D9 because the coefficients of the terms are negative when these drugs combine with our desirable candidates (D3|D6, D4|D9, D7|D9). Note that it is premature to conclude any synergism, antagonism and additive effects simply by looking at the two drug terms. This issue will be discussed at the end of this section.

1st iteration (2nd attempt) with 14 Drug Candidates

Based on the negative coefficients (estimates) and non-significant p values (>0.05), we can eliminate D1, D5, and D10 (Thalidomide, AMD3100, Actinomycin D) [Fig. B7]. Desirable drug candidates have positive coefficients and are significant at the 5% level. They are D4, D6, D7, D11, D13 and D14 (Zoledronic Acid, Bortezomib, Carfilzomib, Mitomycin C, Panobinostat, Dexamethasone). D2, D3, D11 (Lenalidomide, Cyclophosphamide monohydrate, Mitomycin C) are inconclusive. Examining two drug terms, we can eliminate D3 and D11 because the coefficients of these terms are negative when these drugs (D3 and D11) combine with our desirable candidates (D3|D8, D7|D11, D11|D14).

The favorable drugs from the 1st attempt are D4, D6, D7, D11, D13 and D14 while the favorable drugs from the 2nd attempt are D6, D7, D8, D9, D12, D13 and D14. The similar drugs in these two sets are D6, D7, D13 and D14 (Bortezomib, Carfilzomib, Panobinostat and Dexamethasone). Interestingly, these four drugs will be selected for the third iteration. We decide to combine the drugs in these two sets for the second iteration: D4, D6, D7, D8, D9, D11, D12, D13 and D14 (Zoledronic acid, Bortezomib, Carfilzomib, Mechloerthamine HCl, Decitabine, Mitomycin C, Doxorubicin, Panobinostat, Dexamethasone) .

2nd iteration with 9 Drug Candidates

D7, D13, D14 are desirable candidates (Carfilzomib, Panobinostat, Dexamethasone). D11 (Mitomycin C) should be removed based on its negative coefficient and insignificant p value (>0.05) [Fig. B8]. While D6 (Bortezomib) has a negative coefficient at the single drug level, the two-drug and squared terms ($D6|D7$ and $D6^2$) are highly positive and significant. Moreover, Bortezomib has been shown to be highly favorable in the first iteration experiments. D9 (Decitabine) should be removed because it negatively combines with D13 and D14. D4 (Zoledronic acid) negatively combines with D14 while D12 (Doxorubicin) negatively combines with D7. Hence, we eliminate both D4 and D12. D8 (Mechloroethamine HCl) presents a relatively small positive coefficient and is thus inconclusive. We decide to retain D8 for the third iteration.

3rd iteration with 5 Drug Candidates

The fitting correlation and the adjusted R-squared values are high (88.8% and 77.4%), which means the equation accounts for a high variability in the output [Fig. B9]. Even though D6 (Bortezomib) has a negative drug effect (-6.441) at the single drug level, the squared term ($D6^2$) has a markedly positive effect (+94420). Hence, D6 should be retained in the combination. Note that the p values for individual terms D6 (Bortezomib), D7 (Carfilzomib) and D8 (Mech HCl) are not significant at the 5% significance level ($p>0.05$). The significant two-drug term of D6 and D7 has a highly negative coefficient (-1563). D13 (Panobinostat) and D14 (Dexamethasone) are significant and highly positive terms. Together with D6 (Bortezomib), these form our ideal drug candidates. At this iteration, we are interested in determining the right drug concentrations *in vitro*, unlike the previous iterations of drug screening. The MATLAB

output contains a full list of 3125 combinations and their respective outputs [Fig. B11] based on the linear regression experimental process [Fig. B9]. The list is created using various drug concentrations (IC8.75 to IC35) of all the five different drugs.

The set of four diagnostic plots for this 3rd iteration are also shown in Fig. B10. MATLAB generates these diagnostic plots for each iteration. In addition to the fitting correlation and adjusted R^2 values, these plots provide additional evidence for the strength of data fitting by the linear regression experimental process.

In Fig. B10a “Plot of residuals vs fitted values”, we see random and evenly distributed data points along the horizontal 0 line. This indicates a homoscedastic linear model with normally distributed errors. Homoscedasticity means that the variance is homogenous. The standard deviation of output y is independent of the predictor x terms.

The dashed line in the Cook’s distance plot is the recommended threshold value for outliers [Fig. B10 b]. Data points with Cook’s distance exceeding this line could be outliers which can markedly skew the linear regression model. Observations 4 and 32 have relatively larger Cook’s distance than the other 6 observations. It is unnecessary to remove these outliers because the fitting correlation is a high of 88.9%. Removing both outliers will result in a similar linear regression experimental process and marginal improvement in the fitting correlation.

The y axis for the “Normality probability plot” has been scaled such that a normal distribution would fall on the diagonal straight line [Fig. B10 c]. The plots fall on the straight line indicating that the variance is normally distributed.

The histogram of residuals shows a bell-shaped pattern which indicates a normally distributed variance [Fig. B10 d]. These graphs indicate that the residuals are randomly distributed around zero and are independent of the variables.

Prescribed and Empirically Validated Top Combinations

The ten best and ten worst performing two-drug or three-drug combinations were selected from the list of 3125 combinations. *In vitro* validation experiments were then performed [Fig. B12 a]. We avoided four-drug and five-drug combinations because additive effects can confound the data. Adding one drug to the mix can improve the output even though the drug does not create any synergy.

This excerpt of twenty top prescribed combinations shows us that Bortezomib, Panobinostat and Dexamethasone should be kept at high concentrations [Fig. B11]. Carfilzomib is clearly the least favorable candidate. By selecting the top 10 combinations consisting of only two or three drugs [Fig. B12 a], we can conclude that a three-drug prescribed combination would be Bortezomib, Panobinostat and Dexamethasone.

If only two drugs are available, they should be Bortezomib and Dexamethasone. This is combination number 12th and 12th in rank after verification experiments [Fig. B12 a]. This pair is the only 2-drug combination in the list of top 10 [Fig. B12 a] and their concentrations are always kept high at IC35. When we add Panobinostat and gradually increase its concentration, the prescribed output (no. 12, 15, 18, 19, 20) increases. Similarly, the experimental output, except for the bottom two combinations, increases (rank 12, 11, 16, 19, 20). Mechloroethamine would be the 4th choice of drug judging from the prescribed and experimental output. By increasing

Mechloroethamine concentration, the prescribed ordering increases (no. 12, 13, 14, 16, 17) and the ranking of experimental output increases (rank 12, 13, 14, 15, 18). Overall, the prescribed and experimental rankings show that Panobinostat is a more superior drug compared to Mechloroethamine HCl. Carfilzomib could be removed because its concentration is almost always kept at 0.

The bottom ten and top ten combinations form two clearly distinct regions with very different outputs [Fig. B12 b]. Overall, the range of experimental outputs falls in the range of the prescribed outputs. The verification experiments show that the top ten combinations are more superior than the bottom ten combinations. Pearson correlation, or Pearson product-moment correlation coefficient, measures the strength of the linear relationship between two variables. If the prescribed output correlates 100% positively with the experimental output, then the coefficient is +1. No correlation would be 0 and 100% negative correlation would be -1. The bottom ten combinations have a correlation of +0.403 [Fig. B13 b]. The top ten combinations have a correlation of +0.4597 but upon removal of combination number 11, the correlation improved to a high of +0.887. While the correlation for the bottom combinations are not satisfactory, this could be improved by working with more combinations over a wider range of prescribed output. Moreover, the bottom combinations have prescribed and experimental output values close to 0. At such low values, any random errors made during experiments can markedly change the output values, affect the ranking order and affect the correlation. However, this is our least concern here as we are focused on determining the top working combinations.

Combination Index and Two-Drug Interaction Plots

Drug interactions can be antagonistic, additive or synergistic. In order to truly determine the combination index (CI), new experiments for dose-response curves for drug A individually, drug B individually and both drugs in combination have to be done. The combination index can be calculated using the Chou-Talalay method and the type of drug interaction determined⁵⁴. The Chou-Talalay combination index (CI) equation is shown below⁵⁵.

$$CI = \frac{D_{1c}}{D_1} + \frac{D_{2c}}{D_2}$$

Where D_1 is the concentration of drug A alone required to inhibit a system by x% and D_{1c} is the concentration of drug A necessary when used in combination with another drug. Combination index equals to 1 means an additive effect. CI less than 1 means a synergistic effect. CI greater 1 means an antagonistic effect. Determining the CI of various pairings of drugs in this 3rd iteration can be done in future.

The linear regression experimental process and the two-drug interaction response surface plots are more simplified in the 3rd iteration as compared to the 2nd iteration because these five drug candidates have already been selected towards the optimum combination. There are 36 such graphs (9 drugs) for the second iteration and 10 graphs (5 drugs) for the third iteration. Four Bortezomib drug interaction-plots in the second iteration are presented in Fig. B14. When a drug pair is plotted, the concentrations of the other 7 drugs are kept constant at the median level (IC 12.5). The output is determined using this linear regression experimental process (2nd iteration).

$$\begin{aligned}
y = & \beta_0 + \beta_4 X_4 + \beta_6 X_6 + \beta_7 X_7 + \beta_8 X_8 + \beta_9 X_9 + \beta_{11} X_{11} + \beta_{12} X_{12} + \beta_{13} X_{13} + \beta_{14} X_{14} \\
& + \beta_{4,9} X_4 X_9 + \beta_{4,14} X_4 X_{14} + \beta_{6,7} X_6 X_7 + \beta_{7,12} X_7 X_{12} + \beta_{8,9} X_8 X_9 + \beta_{8,12} X_8 X_{12} + \beta_{9,11} X_9 X_{11} \\
& + \beta_{9,12} X_9 X_{12} + \beta_{9,13} X_9 X_{13} + \beta_{9,14} X_9 X_{14} + \beta_{13,14} X_{13} X_{14} + \beta_{66} X_6^2
\end{aligned}$$

The interaction plot [Fig. B14 a] for Bortezomib (D6) and Carfilzomib (D7) is based on the equation above. The terms which vary are $\beta_6 X_6$, $\beta_7 X_7$, $\beta_{6,7} X_6 X_7$, $\beta_{7,12} X_7 X_{12}$ and $\beta_{66} X_6^2$ while the other terms are constants. While the interaction term $\beta_{6,7} X_6 X_7$ has a positive coefficient [Fig. B8], one cannot simply conclude that the drug interaction is synergistic. Accounting for all the terms involved, the response surface plot shows regions of antagonism and possible synergism judging from the trough (blue) and peak (red). The three other plots [Fig. B14 b c d] also show this coexistence of troughs and peaks. The presence of a trough in each of these four plots shows that while Bortezomib has been identified as a good candidate, the right concentrations should be used for the desired outcome. Otherwise, Bortezomib ($\sim 0.6 \text{E-}3 \mu\text{M}$) could hinder a desired therapeutic outcome. In our laboratory recently, such complex response surfaces plots have previously been formed from studies involving breast cancer cell lines and a different set of nanodiamond-chemotherapeutics⁵². Traditional additive methods of applying drug dosages based on single drug experiments are ineffective because drugs used in combination can behave very differently. Response surface plots can also have both concave and convex regions and conclusions of drug interactions cannot be made simply by looking at the curvature of these surfaces⁵⁶.

While a drug pair is antagonistic given decreasing output with increasing drug concentrations, the reverse is not true. When the output increases with increasing drug concentrations in a drug pair, one should account for additive effects before claiming the interaction is synergistic⁵⁴. In

some cases, the drug pair may even be slightly antagonistic. The combination index should be determined by performing dose-response experiments.

Related Clinical Trials and Conclusions

Norvatis Pharmaceuticals has funded clinical trials to investigate the advantage of adding Panobinostat to the Bortezomib-Dexamethasone drug pair. These three drugs have complementary mechanisms against cancer cells. Bortezomib inhibits the mammalian 26S proteasome, while Panobinostat inhibits multiple histone deacetylase enzymes. Dexamethasone binds to glucocorticoid receptors and subsequently modifies transcription via glucocorticoid response elements.

Paul Richardson et al. conducted two separate clinical trials to evaluate the advantages of the three drug combination – Bortezomib-Panobinostat-Dexamethasone. PANORAMA-1 (PANobinostat ORAI in Multiple Myeloma) clinical study involves 768 patients who had relapsed or relapsed and refractory myeloma⁵⁷. These patients had undergone one to three previous treatment regimens. PANORAMA-2 is a similar study with the focus on heavily pretreated Bortezomib-refractory patients⁵⁸ who have undergone four prior treatment regimens including two Bortezomib-containing regimens.

In PANORAMA-1 at phase III, the median overall survival was 33.64 months for the Panobinostat group vs 30.39 months for the placebo group⁵⁷. Patients with complete or near complete response was significantly better in the Panobinostat group (27.6% vs 15.7%). Data on overall survival is not yet mature. The promising subgroup data resulted in the FDA granting accelerated approval to the inclusion of Panobinostat for relapsed myeloma patients who have

received at least two standard therapies including Bortezomib and an immunomodulatory agent⁵⁹.

In PANORAMA-2 at phase II, patients undergoing this three-drug combination achieved an overall response rate of 34.5% and a clinical benefit rate of 52.7%. The authors concluded that the three drug combination can salvage Bortezomib-resistant patients.

Both research works agree with our conclusion of the best three drug candidates even though our *in vitro* work is focused on Bortezomib-sensitive cancer cells and the clinical work is based largely on Bortezomib-resistant, relapsed and refractory patients.

The dosages used in the PANORAMA are based on maximum tolerated dosages which can cause adverse events and discontinuation of therapy⁶⁰. The adverse events include thrombocytopenia, neutropenia, asthenia and fatigue. During the dose escalation phase, almost half of the patients discontinued therapy. The subsequent expansion phase saw one third of the patients stopping treatment. During phase III of PANORAMA-1, serious adverse events were reported in 60% of patients in the Panobinostat group⁵⁷.

A better alternative to using maximum tolerated dosages would be to use Response Surface Optimization (RSO). As shown earlier in the Bortezomib interaction plots [Fig. B14], higher drug doses do not always lead to better output. Rather, the optimum doses for best therapeutic outcome should be based on the global peaks on the response surface maps. The *in vitro* data can then be scaled up for animal models and clinical trials, such that optimum efficacy and minimum adverse events are achieved.

Notably, this RSO methodology is mechanism-independent. We conducted the experiments on these fourteen drugs without any prior knowledge on drug mechanisms. After isolating Bortezomib-Panobinostat-Dexamethasone as our ideal combination, we realized that these three drugs have complementary pharmacological activities. We achieved this within five months when the typical additive discovery approach would take decades and require huge financial investments. Importantly, RSO is not a modeling or predictive approach. The linear regression experimental process (mathematical equation) reconciles empirical data and rapidly makes interpretations. These conclusions can then be validated in a new set of experiments. This rapid iterative cycle is important in a clinic setting where disease progression and treatment outcomes warrant new effective interventions for patients. This RSO platform can be successfully applied to personalize treatment for each patient suffering from multiple myeloma, breast cancer⁵², and many other diseases.

Figures for
“Lysozyme-Triggered Nanodiamond Contact Lens for Glaucoma Treatment”

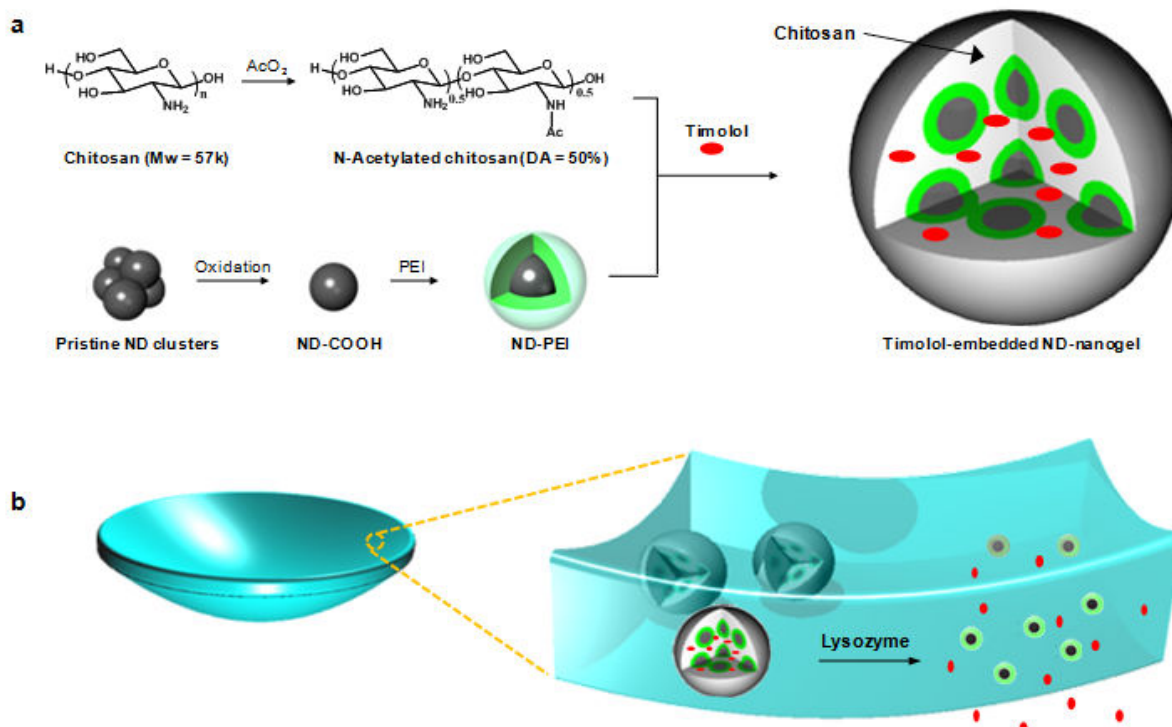


Figure A1: Schematic illustration of our lysozyme-activated drug eluting contact lens. **(a)** Drug-loaded ND-nanogels are synthesized by cross-linking PEI-coated NDs and partially N-acetylated chitosan (MW = 57k, degree of N-acetylation = 50 %) in the presence of timolol maleate. The ND-nanogels are then embedded in a hydrogel and cast into enzyme-responsive contact lenses. **(b)** Exposure to lacrimal fluid lysozyme cleaves the N-acetylated chitosan, degrading the ND-nanogels and releasing the entrapped timolol maleate while leaving the lens intact.

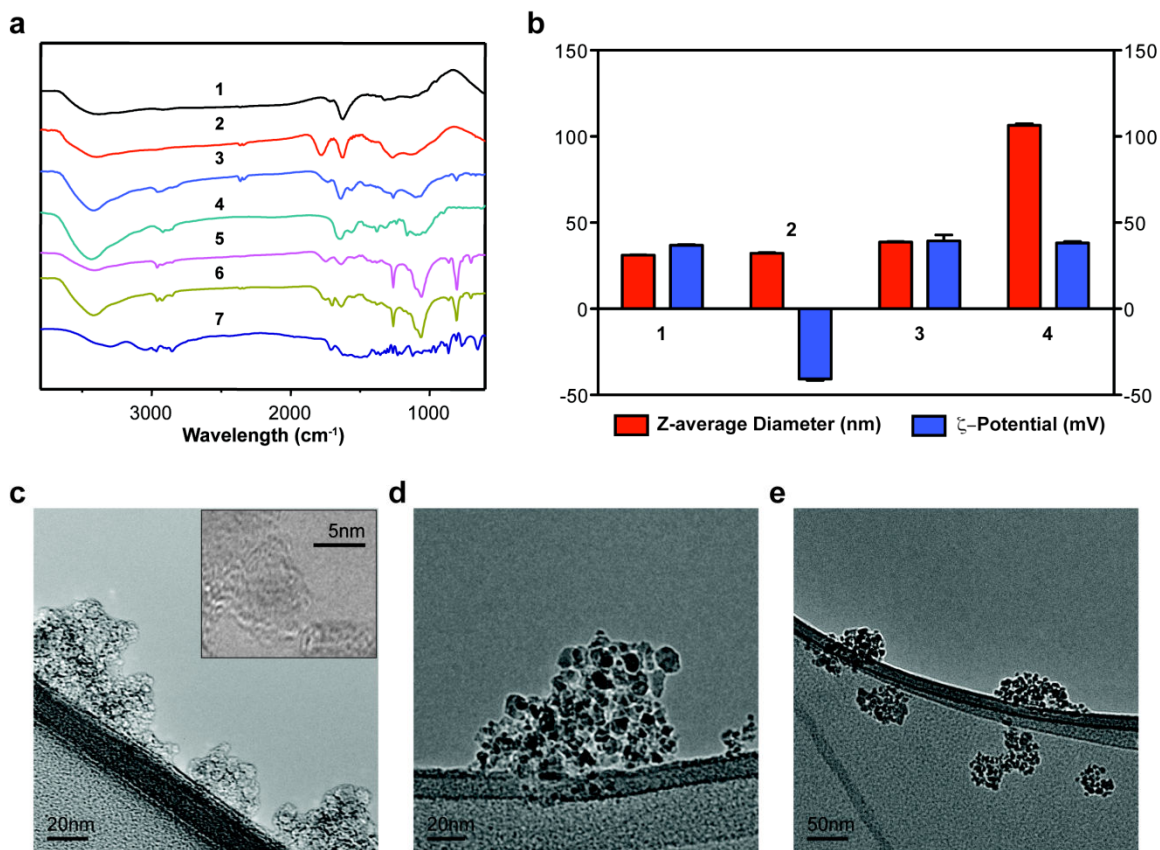


Figure A2: Characterization of ND-nanogel during synthesis. **(a)** FT-IR spectra of (1) pristine ND, (2) oxidized ND, (3) ND-PEI, (4) N-acetylated chitosan, (5) ND-nanogel, (6) timolol (TM) - loaded ND-nanogel, and (7) timolol. **(b)** Particle size (red-colored bars) and ζ potential (blue-colored bars) distributions of (1) pristine ND, (2) oxidized ND, (3) ND-PEI, and (4) TM-loaded ND-nanogel. TEM images of **(c)** pristine ND, **(d)** ND-PEI, and **(e)** TM-loaded ND-nanogel.

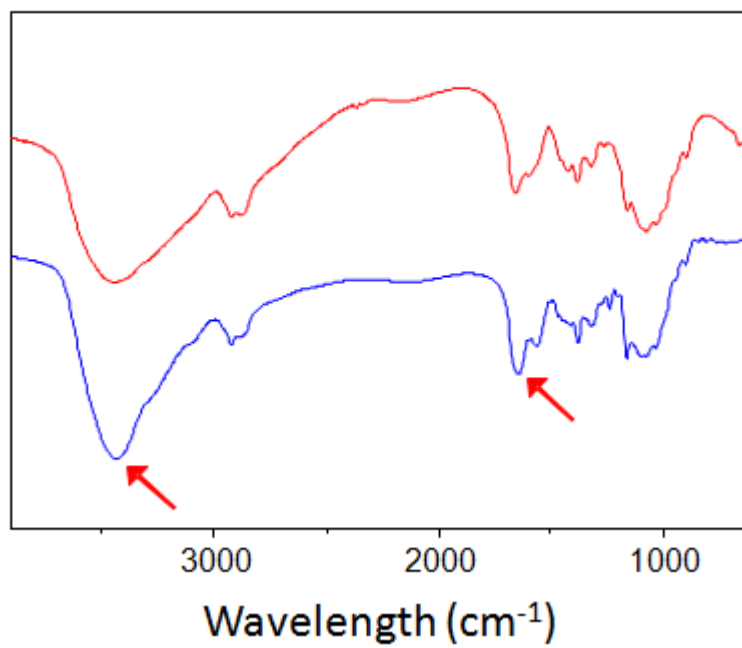


Figure A3: FTIR spectra of chitosan (red) and N-acetylated chitosan (blue). Red arrows indicate the presence of secondary amide bonds in N-acetyl group.

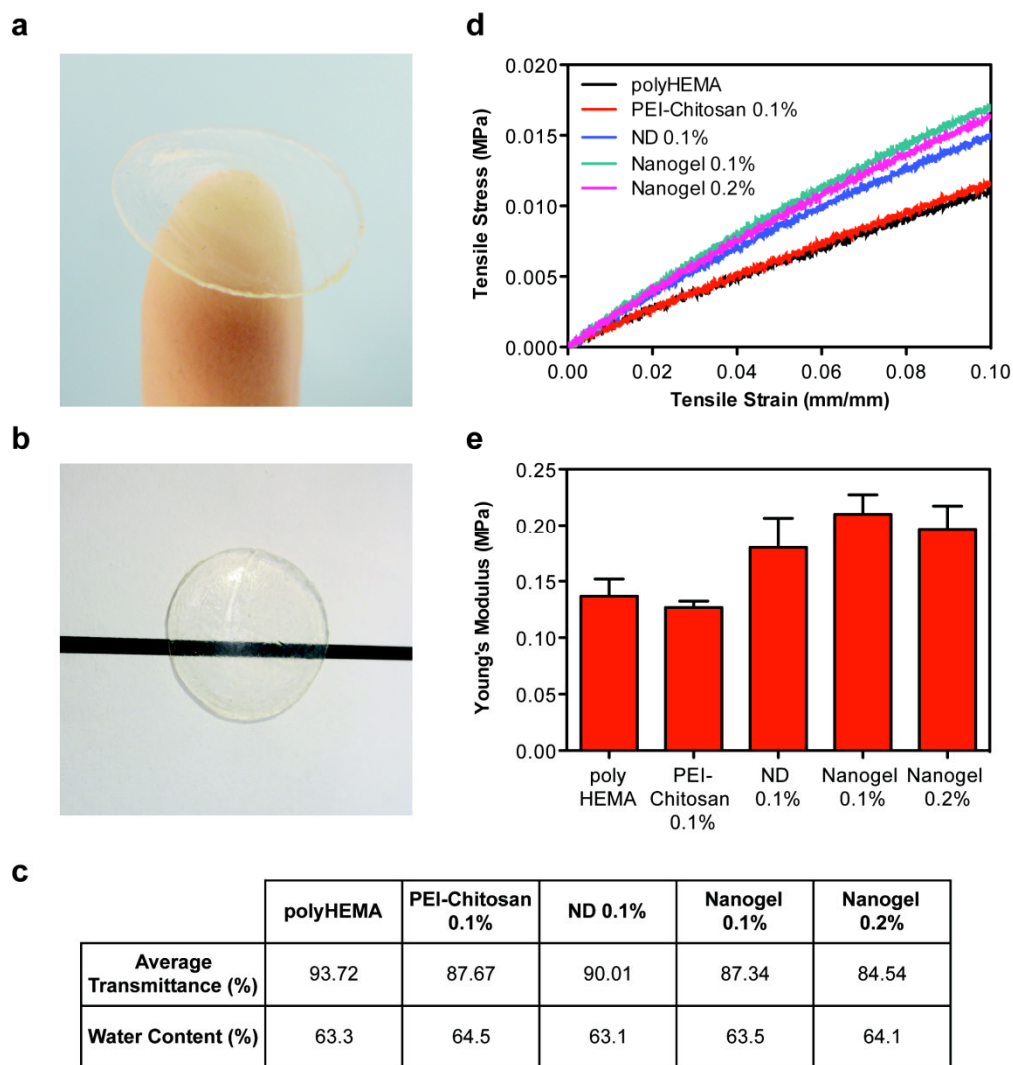


Figure A4: Characterization of physical properties of contact lenses. **(a)** ND-nanogels can be embedded into poly-HEMA gels and cast into contact lenses. **(b)** ND-nanogel embedded lenses maintain optical transparency. **(c)** Comparison of average visible light transmittance (400-700nm) and water content of poly-HEMA lenses without additives, with 0.1% (w/w) PEI-chitosan, with 0.1% (w/w) pristine ND, with 0.1% (w/w) ND-nanogel or 0.2% (w/w) ND-nanogel. **(d)** Tensile stress-strain curves comparing poly-HEMA lenses without additives, with 0.1% (w/w) PEI-chitosan, with 0.1% (w/w) pristine ND, with 0.1% (w/w) ND-nanogel or with 0.2% (w/w) ND-nanogel. **(e)** Young's modulus of the poly-HEMA lenses without additives, with 0.1% (w/w) PEI-chitosan, with 0.1% (w/w) pristine ND, with 0.1% (w/w) ND-nanogel or with 0.2% (w/w) ND-nanogel, as determined by the first 5% of the stress-strain curve slope.

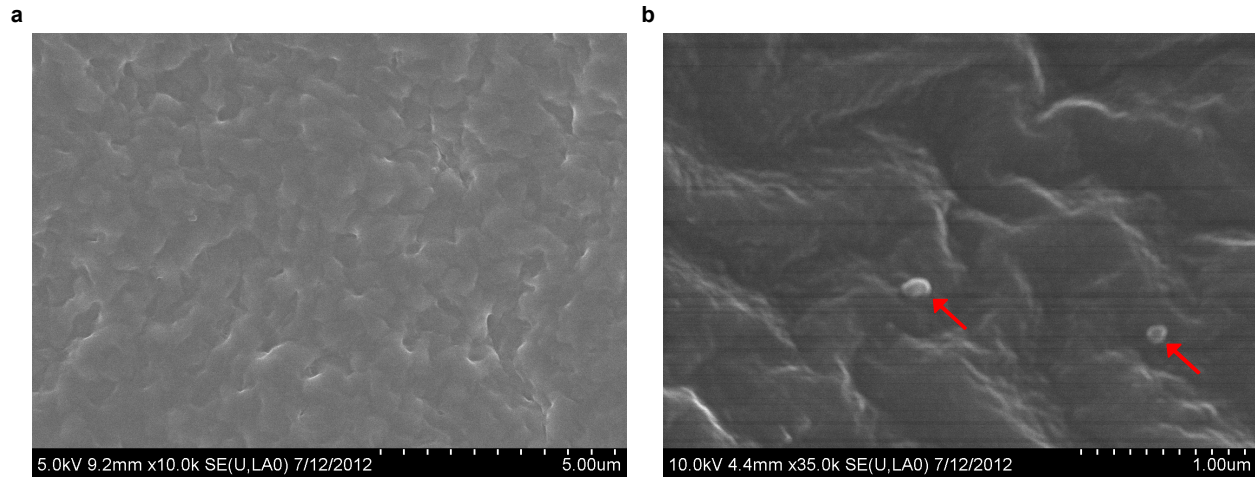


Figure A5: SEM images of (a) Poly-HEMA contact lens and (b) ND-nanogel embedded contact lens at higher magnification. ND-nanogels of approximately 100 nm size were observed on the surface of contact lenses (red arrows).

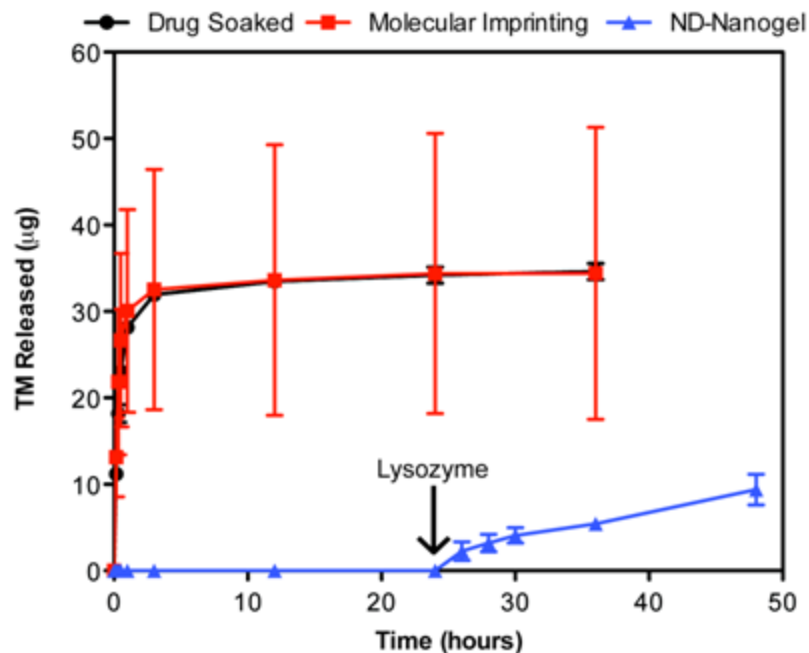


Figure A6: Enzyme-triggered drug release. Drug-eluting profiles from drug-soaked (black line), molecularly-imprinted (red line) and ND nanogel-embedded contact lenses (blue line) in saline solution at 37°C as determined by HPLC analysis of timolol. Lysozyme (2.7mg/mL) in PBS was added at 24 hours incubation (N=3 for each type of lens).

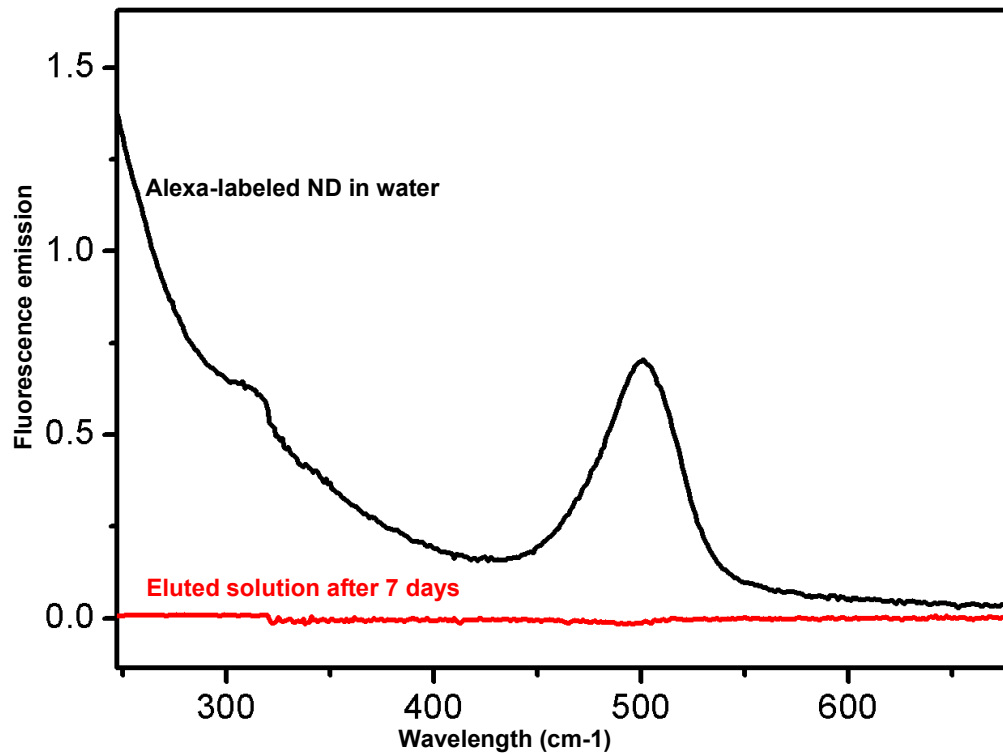


Figure A7: Fluorescence spectral scan of Alexa Fluor® 488-labeled ND in water (black) and eluted solution from ND-nanogel lens over 7 days in lysozyme solution (red). Negligible fluorescence level was detected in the elution after 7 days, indicating an absence of NDs.

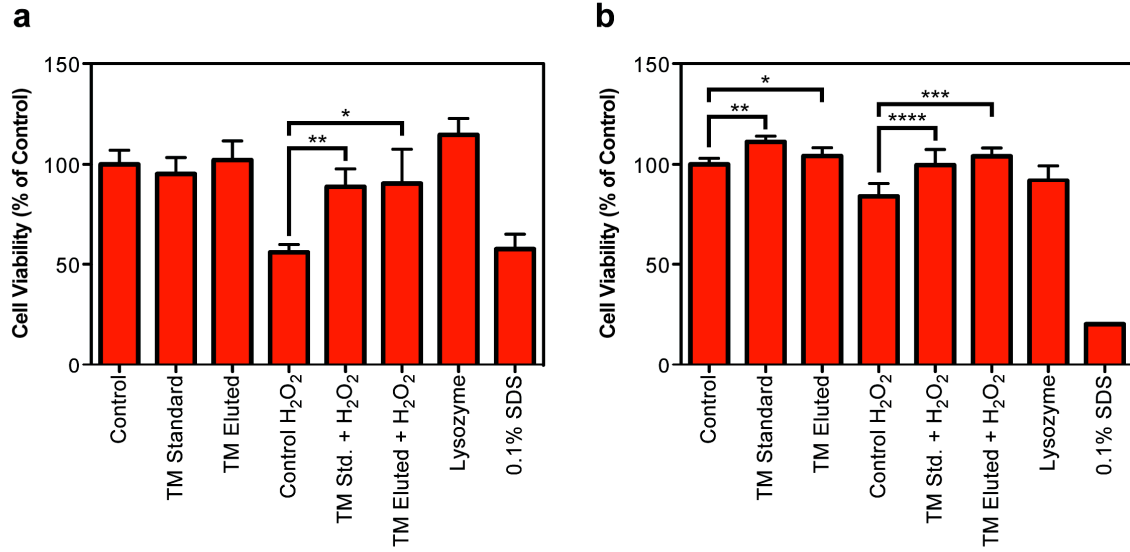


Figure A8: Evaluation of the antioxidant capacity of timolol using primary human trabecular meshwork cells. Cells were treated with control, standard TM or ND-nanogel - eluted TM prior to incubation with 20 μ M H₂O₂ to induce oxidative cell death. **(a)** XTT cell viability assay (N=8; * p=4.2x10⁻⁸, ** p=6.0x10⁻⁵). **(b)** CellTiter-Blue cell viability assay (N=6; * p=0.033, ** p=1.0x10⁻⁶, *** p= 3.3x10⁻⁵, **** p=0.0024).

Figures for
“Phenotypically-based Combinatorial Drug Optimization
for Multiple Myeloma Treatment”

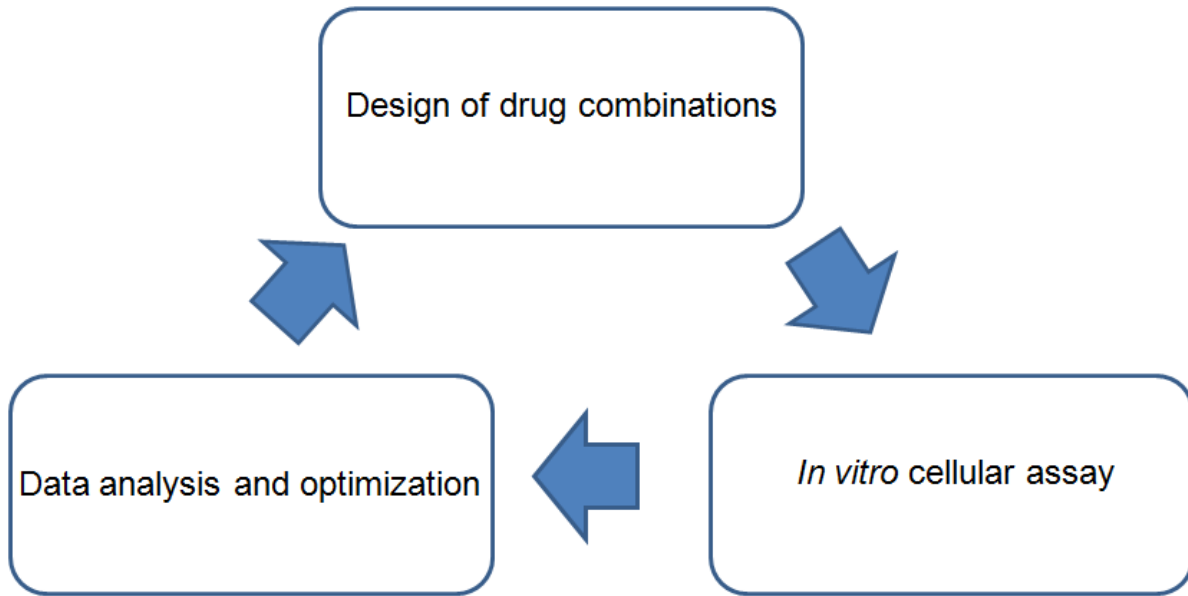


Figure B1: Flowchart showing the three stages of the Response Surface Optimization (RSO) platform for optimizing drug combinations.

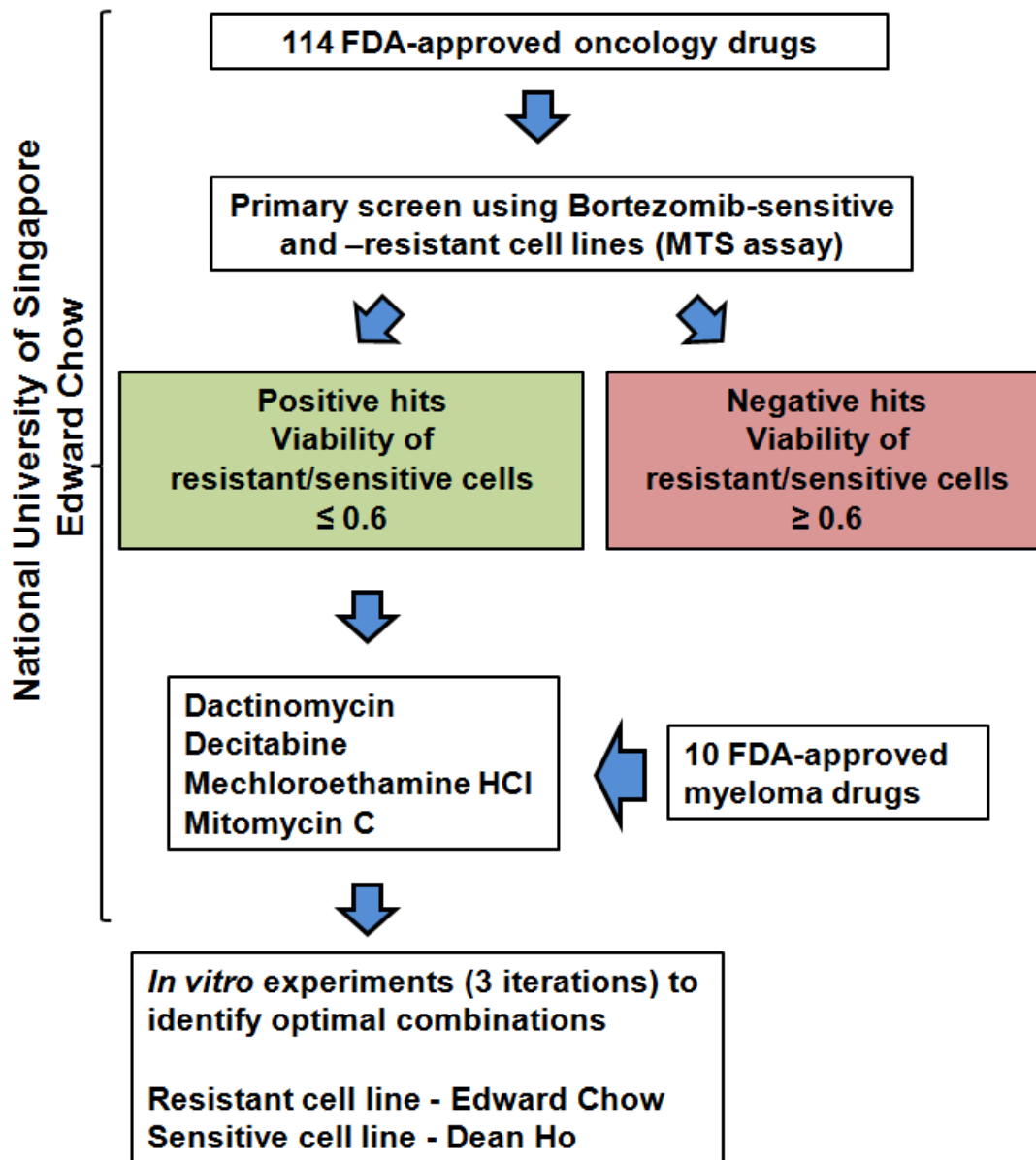


Figure B2: Schematic showing the background of the multiple myeloma collaboration with Professor Edward Chow at the National University of Singapore (NUS). The drug screening process selects for candidates which are more effective in killing the resistant-line than the sensitive-line. The value of 0.6 is set arbitrarily. The four candidates are combined with ten FDA-approved myeloma drugs to make the drug candidates for our first iteration. Dean Ho of UCLA is focused on the Bortezomib-sensitive cell line (RPMI 8226) while Edward Chow of NUS is focused on the Bortezomib-resistant cell line (RPMI 8226p100v).

No.	Zole	Bort	Carf	Mech	Deci	Mito	Doxo	Pano	Dexa
146	0	1	1	1	1	0	-1	-1	-1
147	1	-1	-1	1	1	1	1	-1	1
148	1	-1	0	-1	1	0	-1	1	0
149	1	-1	1	0	1	-1	0	0	-1
150	1	0	-1	-1	0	-1	1	0	0
151	1	0	0	0	0	1	-1	-1	-1
152	1	0	1	1	0	0	0	1	1
153	1	1	-1	0	-1	0	1	1	-1
154	1	1	0	1	-1	-1	-1	0	1
155	1	1	1	-1	-1	1	0	-1	0

Figure B3: An excerpt of the list of drug combinations in the second iteration (experimental run). “-1” and “1” represent the absence or presence of the respective drug in the drug combination. “0” represents an intermediate concentration. The full list of 14 drugs can be found in Figure B5. The drugs here are Zoledronic acid, Bortezomib, Carfilzomib, Mechloroethamine HCl, Decitabine, Mitomycin C, Doxorubicin, Panobinostat and Dexamethasone.

Iteration	No. of Drugs	No. of Combinations	No. of Discrete Levels	Highest Concentration	Other Concentrations
1st	14	128	2	IC 20	0
2nd	9	155	3	IC 25	IC 12.5 0
3rd	5	100	5	IC 35	IC 26.25 IC 17.50 IC 8.75 0

Figure B4: Table showing the design of the three iterations. IC20 represents 20% inhibitory concentration which is the concentration of drug necessary for 20% inhibition of cell growth. The 1st and 2nd iterations are drug screening experiments to remove unfavorable drug candidates. In the 3rd iteration, the goal is to determine the optimum concentrations of the five drugs.

NUMBER	DRUGS
D1	Thalidomide
D2	Lenalidomide
D3	Cyclophosphamide monohydrate
D4	Zoledronic acid
D5	AMD3100
D6	Bortezomib
D7	Carfilzomib
D8	Mechloroethamine HCl
D9	Decitabine
D10	Actinomycin D
D11	Mitomycin C
D12	Doxorubicin
D13	Panobinostat
D14	Dexamethasone



 Drugs removed after 1st iteration
  Drugs removed after 2nd iteration

Figure B5: List of 14 drugs used for the 1st iteration. After the 1st iteration, the drugs highlighted in red were removed. After the 2nd iteration, the drugs highlighted in orange were removed. The remaining five drugs were used for the third iteration (Bortezomib, Carfilzomib, Mechloroethamine HCl, Panobinostat and Dexamethasone).

	Estimate	pValue		Estimate	pValue
Intercept	-0.11238	4.03E-14	D1:D4	-0.02235	-0.02235
D1	0.00521	0.676132	D1:D6	-0.02499	-0.02499
D2	0.012901	0.302158	D1:D9	-0.03503	-0.03503
D3	-0.02228	0.07659	D1:D10	0.047799	0.047799
D4	0.036053	0.004724	D1:D11	-0.04874	-0.04874
D5	-0.01206	0.334476	D1:D12	-0.02479	-0.02479
D6	0.065278	0.00000107	D2:D5	-0.03837	-0.03837
D7	0.054193	0.0000359	D2:D7	-0.02471	-0.02471
D8	0.015543	0.214471	D2:D8	-0.02515	-0.02515
D9	0.00452	0.717001	D2:D10	0.027737	0.027737
D10	-0.00772	0.536277	D2:D12	-0.03061	-0.03061
D11	0.032746	0.009985	D3:D6	-0.04909	-0.04909
D12	-0.00439	0.725036	D3:D13	0.027763	0.027763
D13	0.147691	7.77E-20	D3:D14	0.046333	0.046333
D14	0.03474	0.006395	D4:D6	0.032482	0.032482
			D4:D7	0.03387	0.03387
			D4:D9	-0.02346	-0.02346
			D5:D6	0.035033	0.035033
			D5:D8	0.020979	0.020979
			D5:D11	-0.02245	-0.02245
			D5:D14	-0.02648	-0.02648
			D6:D7	0.024502	0.024502
			D7:D8	-0.0461	-0.0461
			D7:D9	-0.04113	-0.04113
			D7:D13	-0.02278	-0.02278
			D7:D14	-0.04043	-0.04043
			D8:D9	-0.02377	-0.02377

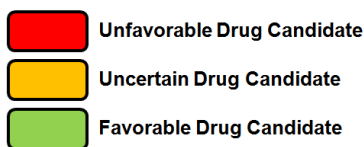


Figure B6: MATLAB multi-drug optimization experimental assessment of first iteration (first attempt) involving 14 drug candidates. Adjusted R^2 : 0.746; Fitting Correlation: 0.91. The adjusted R^2 is 0.746 which means 74.6% of the experiment response can be explained by the linear regression experimental process.

	Estimate	pValue		Estimate	pValue
Intercept	0.273988	2.16E-63	D1:D8	-0.01574	0.014736
D1	-0.00635	0.318547	D2:D3	-0.01478	0.021777
D2	0.004036	0.525611	D2:D5	0.011096	0.083163
D3	0.004492	0.480006	D2:D10	-0.01285	0.04535
D5	-0.00131	0.836503	D2:D12	0.010731	0.093619
D6	0.069822	1.45E-18	D2:D13	0.015142	0.018855
D7	0.085405	1.34E-23	D3:D5	0.011161	0.08139
D8	0.040639	5.82E-09	D3:D8	-0.01781	0.00602
D9	0.020208	0.00194	D3:D12	0.020733	0.001496
D10	-0.00485	0.446083	D3:D13	0.013126	0.041032
D11	0.007133	0.263065	D5:D9	0.017359	0.007361
D12	0.017882	0.005822	D6:D7	0.034436	4.37E-07
D13	0.100244	4.01E-28	D6:D12	-0.01831	0.004785
D14	0.027009	0.0000483	D6:D13	-0.02202	0.000777
			D7:D9	-0.0109	0.088765
			D7:D11	-0.01132	0.077201
			D7:D13	-0.01697	0.008757
			D8:D13	-0.014	0.029531
			D9:D13	-0.0135	0.035681
			D10:D13	0.012068	0.059865
			D11:D14	-0.01884	0.003746

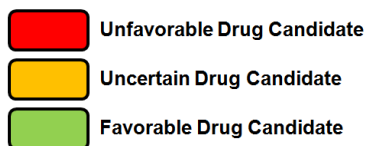


Figure B7: MATLAB multi-drug optimization experimental assessment of first iteration (second attempt) involving 14 drug candidates. Adjusted R-Squared: 0.855; Fitting Correlation: 0.9453. This means 85.5% of the experiment response can be explained by the linear regression experimental process.

	Estimate	pValue
Intercept	-0.13929	8.63E-07
D4	0.004999	0.000857
D6	-125.385	0.056159
D7	26.11804	0.008429
D8	0.026207	6.81E-05
D9	0.759166	1.23E-05
D11	-0.0258	0.320527
D12	8.689137	2.77E-05
D13	70.28295	8.41E-13
D14	23.89866	0.000994
D4:D9	0.015739	0.082187
D4:D14	-1.36845	0.006994
D6:D7	31733.01	4.21E-07
D7:D12	-1815.14	0.046915
D8:D9	-0.08268	0.03226
D8:D12	-1.03035	0.090532
D9:D11	0.436189	0.02472
D9:D12	-26.993	0.009451
D9:D13	-149.008	0.00671
D9:D14	-95.1596	0.00993
D13:D14	5139.906	0.092677
D6^2	80914.41	0.01918

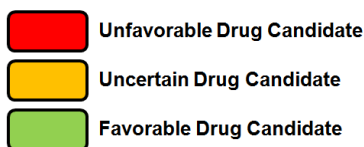


Figure B8: Multi-drug optimization experimental assessment for the 2nd iteration with 9 drug candidates. Adjusted R-Squared 0.734; Fitting correlation is 0.877. This means 73.4% of the experiment response can be explained by the linear regression experimental process.

	Estimate	pValue
Intercept	-1.167E-01	2.100E-02
D6	-6.441E+00	9.006E-01
D7	1.306E+00	2.091E-01
D8	8.008E-02	8.965E-02
D13	9.779E+01	3.624E-04
D14	1.312E+02	3.505E-21
D6:D7	-1.563E+03	2.533E-02
D6^2	9.442E+04	9.361E-07

Linear regression experimental process:

$$y = \beta_0 + \beta_6 X_6 + \beta_7 X_7 + \beta_8 X_8 + \beta_{13} X_{13} + \beta_{14} X_{14} + \beta_{67} X_6 X_7 + \beta_{66} X_6^2$$

Figure B9: Multi-drug optimization experimental assessment for the 3rd iteration with 5 drug candidates. Adjusted R-Squared: 0.774. Fitting Correlation: 0.88873. The adjusted R² is 0.774 which means 77.4% of the experiment response can be explained by the linear regression experimental process.

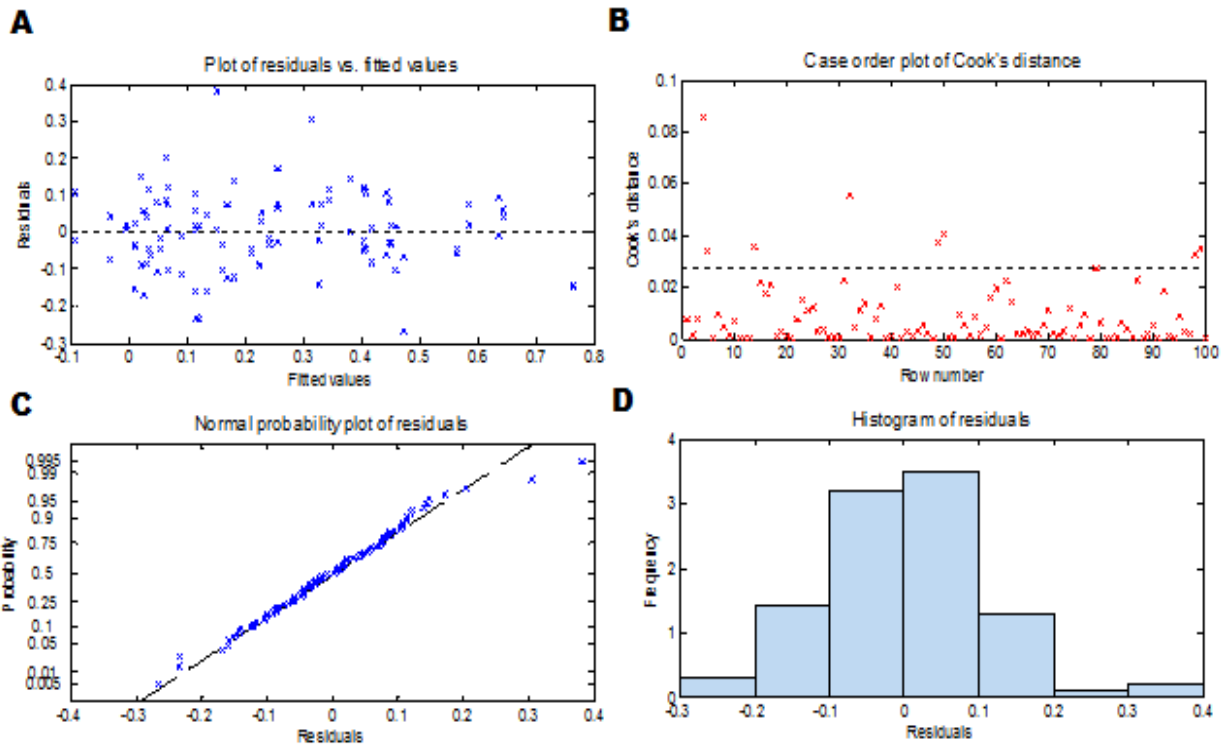


Figure B10: Four diagnostic plots generated specifically for the third iteration. These plots provide information regarding normality of the variance and the strength of the data fitting.

Bort	Carf	Mech	Pano	Dexa	Output
35	0	0	17.5	35	0.8108
35	8.75	26.25	35	35	0.8122
35	17.5	35	35	35	0.81401
35	0	26.25	8.75	35	0.82154
35	0	8.75	17.5	35	0.82215
35	8.75	35	35	35	0.82875
35	0	17.5	17.5	35	0.83394
35	0	35	8.75	35	0.83809
35	0	0	26.25	35	0.83847
35	0	26.25	17.5	35	0.84761
35	0	8.75	26.25	35	0.84982
35	0	17.5	26.25	35	0.86161
35	0	35	17.5	35	0.86416
35	0	0	35	35	0.86988
35	0	26.25	26.25	35	0.87528
35	0	8.75	35	35	0.88123
35	0	35	26.25	35	0.89183
35	0	17.5	35	35	0.89302
35	0	26.25	35	35	0.90669
35	0	35	35	35	0.92324

Figure B11: Excerpt of the top 20 prescribed combinations in a multi-drug optimization experimental assessment. The entire list contains 3125 prescribed combinations and outputs based on the linear regression experimental process [Figure B9]. All the five concentration levels (described in Figure B4) are added into the respective X terms. Here, 35 means IC35 (inhibitory concentration) of that specific drug. The calculated Y from the equation [Figure B9] is the output as shown here. Bort – Bortezomib, Carf – Carfilzomib, Mech – Mechloroethamine HCl, Pano – Panobinostat, Dex – Dexamethasone.

A		Bort	Carf	Mech	Pano	Dexa	Exp Rank	Prescribed Output	Experimental Output
Bottom 10	1	0	0	8.75	0	8.75	2	-0.1044	0.0158
	2	0	0	17.5	0	8.75	4	-0.0926	0.0533
	3	0	0	8.75	0	17.5	5	-0.0910	0.0631
	4	0	0	0	8.75	8.75	8	-0.0841	0.1850
	5	0	0	17.5	0	17.5	1	-0.0792	-0.0161
	6	0	0	26.25	0	8.75	7	-0.0790	0.1569
	7	0	0	8.75	8.75	0	6	-0.0737	0.1360
	8	0	0	8.75	8.75	8.75	9	-0.0728	0.1908
	9	0	0	0	8.75	17.5	10	-0.0706	0.2214
	10	0	0	26.25	0	17.5	3	-0.0655	0.0253
Top 10	11	35	8.75	0	0	35	17	0.6586	0.6833
	12	35	0	0	0	35	12	0.7531	0.5839
	13	35	0	8.75	0	35	13	0.7644	0.5929
	14	35	0	17.5	0	35	14	0.7762	0.6423
	15	35	0	0	8.75	35	11	0.7847	0.5474
	16	35	0	26.25	0	35	15	0.7899	0.6627
	17	35	0	35	0	35	18	0.8064	0.7093
	18	35	0	0	17.5	35	16	0.8108	0.6788
	19	35	0	0	26.25	35	19	0.8385	0.7334
	20	35	0	0	35	35	20	0.8699	0.7816

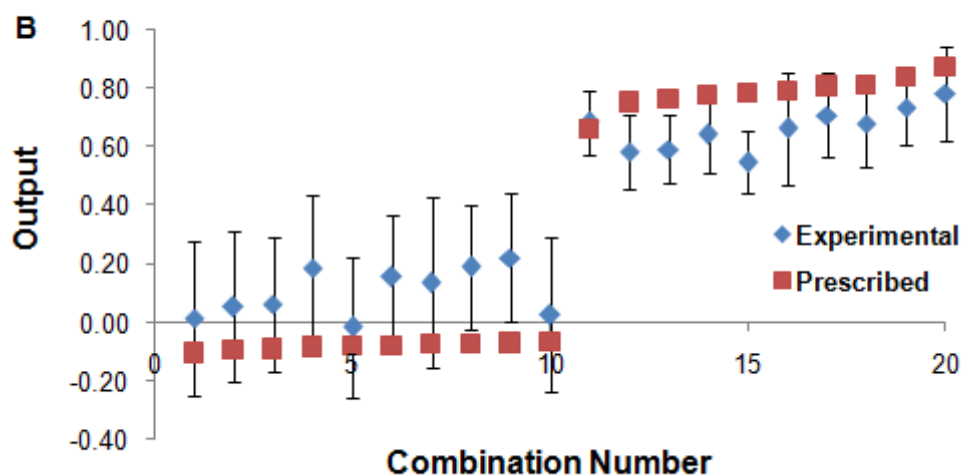


Figure B12 a: Excerpt of the top 10 and bottom 10 prescribed combinations consisting of two or three drugs. These are the combinations selected for *in vitro* experimental verification. The combination ordering is based on ascending prescribed output order. The experimental output is obtained from *in vitro* verification experiments and the “Exp Rank” refers to the rank based on ascending experimental output. Rank number 20 is the best and rank number 1 is the worst. Bort – Bortezomib, Carf – Carfilzomib, Mech – Mechloroethamine HCl, Pano – Panobinostat, Dex – Dexamethasone.

b: Graph showing the experimental and prescribed outputs for the selected combinations.

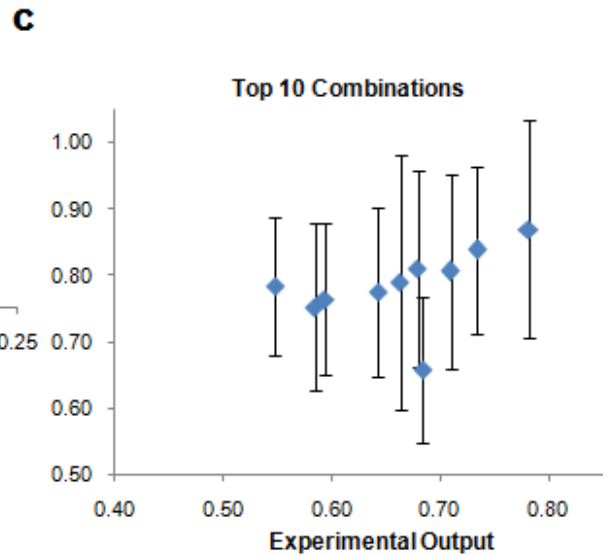
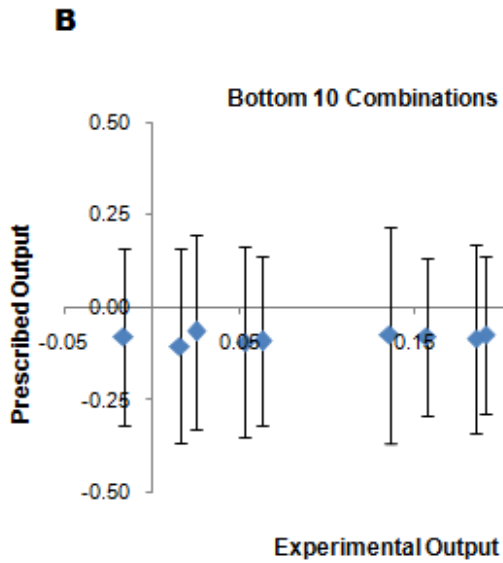
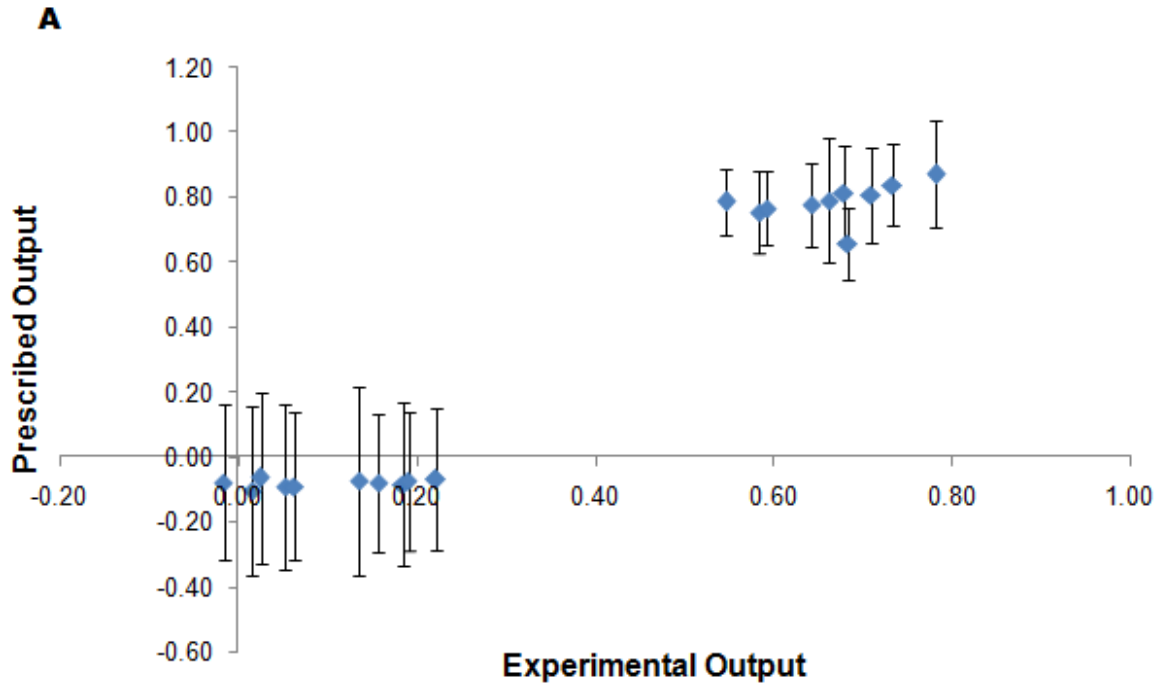


Figure B13: Pearson correlation plots for prescribed outputs vs experimental outputs. Zoomed-in versions of graph A are presented in graphs B and C. The respective Pearson correlations are discussed in the text.

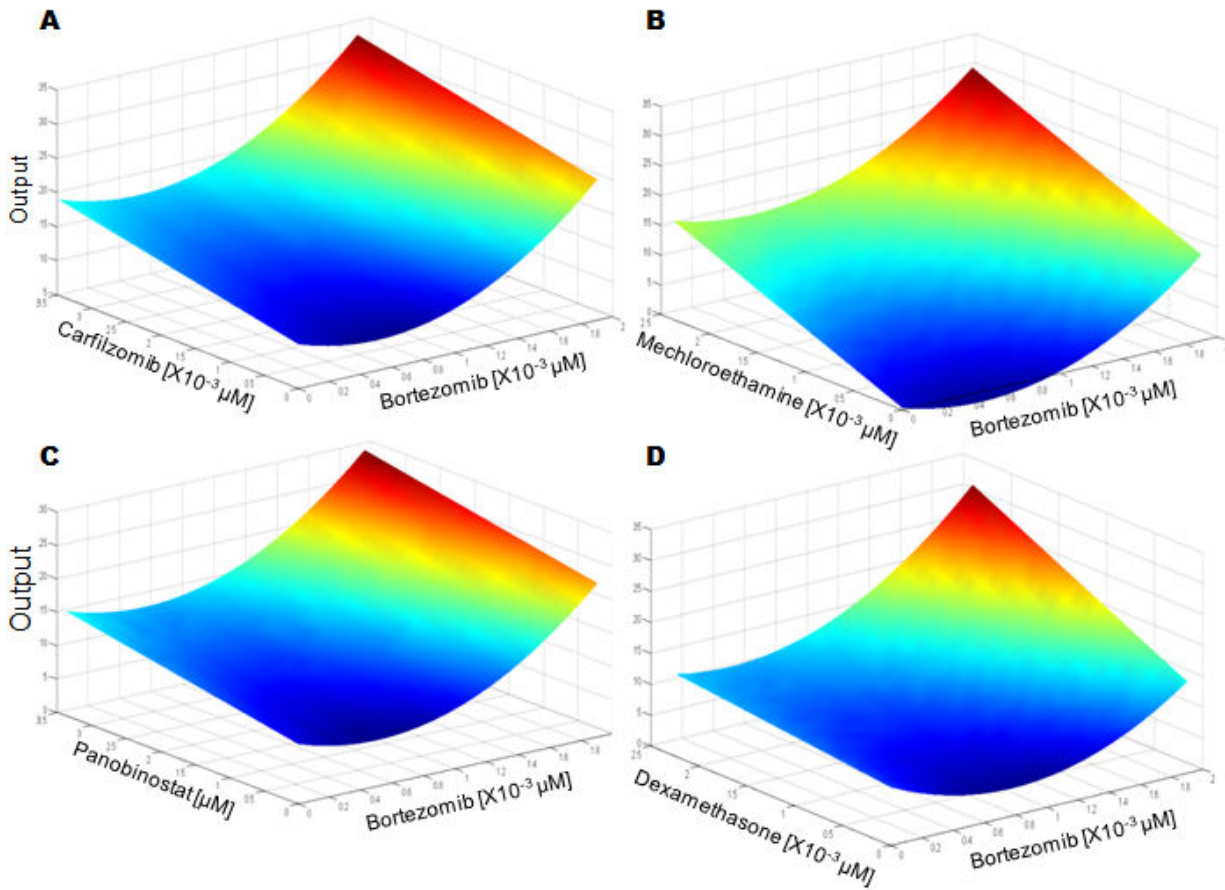


Figure B14: Examples of experimentally-derived response surface plots for the second iteration with nine drugs. These plots vary the concentrations of the two drugs while keeping the other seven drugs constant at their respective median concentrations of IC12.5 [refer Fig B4]. These plots are based on the linear regression experimental process stated in the text.

BIBLIOGRAPHY

- (1) Kim, H. J.; Zhang, K.; Moore, L.; Ho, D. Diamond Nanogel-Embedded Contact Lenses Mediate Lysozyme-Dependent Therapeutic Release. *ACS Nano* **2014**, *8*, 2998–3005.
- (2) Quigley, H. A.; Broman, A. T. The Number of People with Glaucoma Worldwide in 2010 and 2020. *Br. J. Ophthalmol.* **2006**, *90*, 262–267.
- (3) Dreer, L. E.; Girkin, C.; Mansberger, S. L. Determinants of Medication Adherence to Topical Glaucoma Therapy. *J. Glaucoma* **2012**, *21*, 234–240.
- (4) Stryker, J. E.; Beck, A. D.; Primo, S. a; Echt, K. V; Bundy, L.; Pretorius, G. C.; Glanz, K. An Exploratory Study of Factors Influencing Glaucoma Treatment Adherence. *J. Glaucoma* **2010**, *19*, 66–72.
- (5) Sleath, B.; Blalock, S.; Covert, D.; Stone, J. L.; Skinner, A. C.; Muir, K.; Robin, A. L. The Relationship between Glaucoma Medication Adherence, Eye Drop Technique, and Visual Field Defect Severity. *Ophthalmology* **2011**, *118*, 2398–2402.
- (6) Ahmet, E.; Kemal Örnek; Reyhan Güllü; Emel Bulcun; Mehmet Ekici; Ekici, A. Effects of Timolol and Latanoprost on Respiratory and Cardiovascular Status in Elderly Patients with Glaucoma. *J. Ocul. Pharmacol. Ther.* **2009**, *25*, 463–466.
- (7) Wu, S. Y.; Nemesure, B.; Hennis, A.; Schachat, A. P.; Hyman, L. Open-Angle Glaucoma and Mortality. *Arch. Ophthalmol.* **2008**, *126*, 365–370.
- (8) Huang. Physicochemical Properties and In Vivo Assessment of Timolol-Loaded Poly(D,L-Lactide-Co-Glycolide) Films for Long-Term Intraocular Pressure Lowering Effects. *J. Ocul. Pharmacol. Ther.* **2005**, *21*.
- (9) Jung, H. J.; Chauhan, A. Extended Release of Timolol from Nanoparticle-Loaded Fornix Insert for Glaucoma Therapy. *J. Ocul. Pharmacol. Ther.* **2012**, *00*.
- (10) Li, P.-Y.; Shih, J.; Lo, R.; Saati, S.; Agrawal, R.; Humayun, M. S.; Tai, Y.-C.; Meng, E. An Electrochemical Intraocular Drug Delivery Device. *Sensors Actuators A Phys.* **2008**, *143*, 41–48.
- (11) Jung, H. J.; Chauhan, A. Temperature Sensitive Contact Lenses for Triggered Ophthalmic Drug Delivery. *Biomaterials* **2012**, *33*, 2289–2300.
- (12) Alvarez-Lorenzo, C.; Hiratani, H.; Gómez-Amoza, J. L.; Martínez-Pacheco, R.; Souto, C.; Concheiro, A. Soft Contact Lenses Capable of Sustained Delivery of Timolol. *J. Pharm. Sci.* **2002**, *91*, 2182–2192.
- (13) Ali, M. Zero-Order Therapeutic Release from Imprinted Hydrogel Contact Lenses within in Vitro Physiological Ocular Tear Flow. *J. Control. Release* **2007**, *124*.

- (14) Hiratani, H.; Fujiwara, A.; Tamiya, Y.; Mizutani, Y.; Alvarez-Lorenzo, C. Ocular Release of Timolol from Molecularly Imprinted Soft Contact Lenses. *Biomaterials* **2005**, *26*, 1293–1298.
- (15) Ciolino J. B.; Todd R. Hoare; Naomi G. Iwata; Irmgard Behlau; Claes H. Dohlman; Langer, R. A Drug-Eluting Contact Lens. *Invest. Ophthalmol. Vis. Sci.* **2009**, *50*, 3346–3352.
- (16) Ciolino, J. B.; Stefanescu, C. F.; Ross, A. E.; Salvador-Culla, B.; Cortez, P.; Ford, E. M.; Wymbs, K. a; Sprague, S. L.; Mascoop, D. R.; Rudina, S. S.; *et al.* In Vivo Performance of a Drug-Eluting Contact Lens to Treat Glaucoma for a Month. *Biomaterials* **2014**, *35*, 432–439.
- (17) Aimetti, A. A.; Machen, A. J.; Anseth, K. S. Poly(ethylene Glycol) Hydrogels Formed by Thiol-Ene Photopolymerization for Enzyme-Responsive Protein Delivery. *Biomaterials* **2009**, *30*, 6048–6054.
- (18) Ensign, L. M.; Tang, B. C.; Wang, Y.-Y.; Tse, T. A.; Hoen, T.; Cone, R.; Hanes, J. Mucus-Penetrating Nanoparticles for Vaginal Drug Delivery Protect against Herpes Simplex Virus. *Sci. Transl. Med.* **2012**, *4*, 138ra79.
- (19) Hrkach, J.; Von Hoff, D.; Mukkaram Ali, M.; Andrianova, E.; Auer, J.; Campbell, T.; De Witt, D.; Figa, M.; Figueiredo, M.; Horhota, A.; *et al.* Preclinical Development and Clinical Translation of a PSMA-Targeted Docetaxel Nanoparticle with a Differentiated Pharmacological Profile. *Sci. Transl. Med.* **2012**, *4*, 128ra39.
- (20) Kam, K. R.; Walsh, L. A.; Bock, S. M.; Koval, M.; Fischer, K. E.; Ross, R. F.; Desai, T. A. Nanostructure-Mediated Transport of Biologics across Epithelial Tissue: Enhancing Permeability via Nanotopography. *Nano Lett.* **2013**, *13*, 164–171.
- (21) Diebold, Y.; Calonge, M. Applications of Nanoparticles in Ophthalmology. *Prog. Retin. Eye Res.* **2010**, *29*, 596–609.
- (22) Chang, L. Y.; Osawa, E.; Barnard, A. S.; Ōsawa, E. Confirmation of the Electrostatic Self-Assembly of Nanodiamonds. *Nanoscale* **2011**, *3*, 958–962.
- (23) Zhang, Q.; Mochalin, V. N.; Neitzel, I.; Hazeli, K.; Niu, J.; Kotsos, A.; Zhou, J. G.; Lelkes, P. I.; Gogotsi, Y. Mechanical Properties and Biomineralization of Multifunctional Nanodiamond-PLLA Composites for Bone Tissue Engineering. *Biomaterials* **2012**, *33*, 5067–5075.
- (24) Bradac, C.; Gaebel, T.; Naidoo, N.; Sellars, M. J.; Twamley, J.; Brown, L. J.; Barnard, A. S.; Plakhotnik, T.; Zvyagin, A. V.; Rabeau, J. R. Observation and Control of Blinking Nitrogen-Vacancy Centres in Discrete Nanodiamonds. *Nat. Nanotechnol.* **2010**, *5*, 345–349.
- (25) Hartmann, M.; Betz, P.; Sun, Y.; Gorb, S. N.; Lindhorst, T. K.; Krueger, A. Saccharide-Modified Nanodiamond Conjugates for the Efficient Detection and Removal of Pathogenic Bacteria. *Chemistry* **2012**, *18*, 6485–6492.

- (26) Chow, E. K.; Zhang, X.-Q.; Chen, M.; Lam, R.; Robinson, E.; Huang, H.; Schaffer, D.; Osawa, E.; Goga, A.; Ho, D. Nanodiamond Therapeutic Delivery Agents Mediate Enhanced Chemoresistant Tumor Treatment. *Sci. Transl. Med.* **2011**, *3*, 73ra21.
- (27) Moore, L.; Chow, E. K.-H.; Osawa, E.; Bishop, J. M.; Ho, D. Diamond-Lipid Hybrids Enhance Chemotherapeutic Tolerance and Mediate Tumor Regression. *Adv. Mater.* **2013**, *25*, 3532–3541.
- (28) Zhang, X.; Hu, W.; Li, J.; Tao, L.; Wei, Y. A Comparative Study of Cellular Uptake and Cytotoxicity of Multi-Walled Carbon Nanotubes, Graphene Oxide, and Nanodiamond. *Toxicol. Res. (Camb)*. **2012**, *1*, 62–68.
- (29) Chow, E. K.; Zhang, X.-Q.; Chen, M.; Lam, R.; Robinson, E.; Huang, H.; Schaffer, D.; Osawa, E.; Goga, A.; Ho, D. Nanodiamond Therapeutic Delivery Agents Mediate Enhanced Chemoresistant Tumor Treatment. *Sci. Transl. Med.* **2011**, *3*, 73ra21.
- (30) Miyawaki, J.; Yudasaka, M.; Azami, T.; Kubo, Y.; Iijima, S. Toxicity of Single-Walled Carbon Nanohorns. *ACS Nano* **2008**, *2*, 213–226.
- (31) Mochalin, V. N.; Neitzel, I.; Etzold, B. J. M.; Peterson, A.; Palmese, G.; Gogotsi, Y. Covalent Incorporation of Aminated Nanodiamond into an Epoxy Polymer Network. *ACS Nano* **2011**, *5*, 7494–7502.
- (32) Lam R Pierstorff E, Huang H, Osawa E, Ho D, C. M. Nanodiamond-Embedded Microfilm Devices for Localized Chemotherapeutic Elution. *ACS Nano* **2008**, *2*, 2095–2102.
- (33) Ang, P. K.; Loh, K. P.; Wohland, T.; Nesladek, M.; Van Hove, E. Supported Lipid Bilayer on Nanocrystalline Diamond: Dual Optical and Field-Effect Sensor for Membrane Disruption. *Adv. Funct. Mater.* **2009**, *19*, 109–116.
- (34) Li, C.-C.; Huang, C.-L. Preparation of Clear Colloidal Solutions of Detonation Nanodiamond in Organic Solvents. *Colloids Surfaces A Physicochem. Eng. Asp.* **2010**, *353*, 52–56.
- (35) Ren, D.; Yi, H.; Wang, W.; Ma, X. The Enzymatic Degradation and Swelling Properties of Chitosan Matrices with Different Degrees of N-Acetylation. *Carbohydr. Res.* **2005**, *340*, 2403–2410.
- (36) Garrett. Hydrogel Lens Monomer Constituents Modulate Protein Sorption. *Invest. Ophthalmol. Vis. Sci.* **2000**, *41*.
- (37) Osswald, S.; Yushin, G.; Mochalin, V.; Kucheyev, S. O.; Gogotsi, Y. Control of sp(2)/sp(3) Carbon Ratio and Surface Chemistry of Nanodiamond Powders by Selective Oxidation in Air. *J. Am. Chem. Soc.* **2006**, *128*, 11635–11642.
- (38) Li CC, H. C. L. Preparation of Clear Colloidal Solutions of Detonation Nanodiamond in Organic Solvents. *Colloids Surfaces A Physicochem. Eng. Asp.* **2010**, *353*, 52–56.

- (39) Peng, C.-C.; Burke, M. T.; Carbia, B. E.; Plummer, C.; Chauhan, A. Extended Drug Delivery by Contact Lenses for Glaucoma Therapy. *J. Control. Release* **2012**, *162*, 152–158.
- (40) Saccà, S. C.; La Maestra, S.; Micale, R. T.; Larghero, P.; Travaini, G.; Baluce, B.; Izzotti, A. Ability of Dorzolamide Hydrochloride and Timolol Maleate to Target Mitochondria in Glaucoma Therapy. *Arch. Ophthalmol.* **2011**, *129*, 48–55.
- (41) Rajakumar, V.; Kyle, R. Multiple Myeloma: Diagnosis and Treatment. *Mayo Clin. Proc.* **2005**, *80*, 1371–1382.
- (42) Rajkumar, S. V. Treatment of Multiple Myeloma. *Nat. Rev. Clin. Oncol.* **2011**, *8*, 479–491.
- (43) SEER Stat Fact Sheets: Myeloma. *Natl. Cancer Inst. Surveillance, Epidemiol. End Results Progr.* **2015**.
- (44) Richardson, P. G.; Weller, E.; Lonial, S.; Jakubowiak, A. J.; Jagannath, S.; Raje, N. S.; Avigan, D. E.; Xie, W.; Ghobrial, I. M.; Schlossman, R. L.; *et al.* Lenalidomide , Bortezomib , and Dexamethasone Combination Therapy in Patients with Newly Diagnosed Multiple Myeloma. *Blood* **2010**, *116*, 679–686.
- (45) Kumar, S.; Flinn, I.; Richardson, P. G.; Hari, P.; Callander, N.; Noga, S. J.; Stewart, a K.; Turturro, F.; Rifkin, R.; Wolf, J.; *et al.* Randomized , Multicenter , Phase 2 Study (EVOLUTION) of Combinations of Bortezomib , Dexamethasone , Cyclophosphamide , and Lenalidomide in Previously Untreated Multiple Myeloma. *Blood* **2012**, *119*, 4375–4382.
- (46) Hood, L.; Heath, J. R.; Phelps, M. E.; Lin, B. Systems Biology and New Technologies Enable Predictive and Preventative Medicine. *Science (80-.)*. **2004**, *306*, 640–643.
- (47) Al-Lazikani, B.; Banerji, U.; Workman, P. Combinatorial Drug Therapy for Cancer in the Post-Genomic Era. *Nat. Biotechnol.* **2012**, *30*, 679–692.
- (48) Cartier, S.; Zhang, B.; Rosen, V. M.; Zarotsky, V.; Bartlett, J. B.; Mukhopadhyay, P.; Wagner, S.; Davis, C. Relationship between Treatment Effects on Progression-Free Survival and Overall Survival in Multiple Myeloma: A Systematic Review and Meta-Analysis of Published Clinical Trial Data. *Oncol. Res. Treat.* **2015**, *38*, 88–94.
- (49) Kouroukis, T. C.; Baldassarre, F. G.; Haynes, A. E.; Imrie, K.; Reece, D. E.; Cheung, M. C. Bortezomib in Multiple Myeloma : Systematic Review and Clinical Considerations. *Curr. Oncol.* **2014**, *21*, 573–603.
- (50) Drugs Approved for Multiple Myeloma and Other Plasma Cell Neoplasms.
- (51) Yin, N.; Ma, W.; Pei, J.; Ouyang, Q.; Tang, C.; Lai, L. Synergistic and Antagonistic Drug Combinations Depend on Network Topology. *PLoS One* **2014**, *9*.

- (52) Wang, H.; Lee, D.; Chen, K.; Chen, J.; Zhang, K.; Silva, A.; Ho, C.; Ho, D. Mechanism-Independent Optimization of Combinatorial Nanodiamond and Unmodified Drug Delivery Using a Phenotypically Driven Platform Technology. *ACS Nano* **2015**, *9*, 3332–3344.
- (53) Xu, H.; Jaynes, J.; Ding, X. Combining Two-Level and Three-Level Orthogonal Arrays for Factor Screening and Response Surface Exploration. *Stat. Sin.* **2014**, *24*, 269–289.
- (54) Chou, T. C. Drug Combination Studies and Their Synergy Quantification Using the Chou-Talalay Method. *Cancer Res.* **2010**, *70*, 440–446.
- (55) Chou, T. Theoretical Basis , Experimental Design , and Computerized Simulation of Synergism and Antagonism in Drug Combination Studies □. **2007**, *58*, 621–681.
- (56) Murado García, M. A.; Prieto Lage, M. Á. Dose-Response Analysis in the Joint Action of Two Effectors. A New Approach to Simulation, Identification and Modelling of Some Basic Interactions. *PLoS One* **2013**, *8*.
- (57) San-Miguel, J.; Hungria, V.; Yoon, S.-S.; Beksac, M.; Dimopoulos, M.; Elghandour, A. Panobinostat plus Bortezomib and Dexamethasone vs Placebo plus Bortezomib & Dexamethasone in Patients with Relapsed or Relapsed and Refractory Multiple Myeloma: A Multicentre, Randomised, Double-Blinded Phase 3 Trial. *Lancet Oncol.* **2014**, *15*, 1195–1206.
- (58) Richardson, P. G.; Schlossman, R. L.; Alsina, M.; Weber, D. M.; Coutre, S. E.; Gaspardo, C.; Mukhopadhyay, S.; Ondrovik, M. S.; Khan, M.; Paley, C. S.; *et al.* PANORAMA 2: Panobinostat in Combination with Bortezomib and Dexamethasone in Patients with Relapsed and Bortezomib-Refractory Myeloma. *Blood* **2013**, *122*, 2331–2337.
- (59) Nelson, R. FDA Approves Panobinostat for Relapsed Multiple. *Medscape Med. News* **2015**, *Feb 23*.
- (60) San-Miguel, J. F.; Richardson, P. G.; Günther, A.; Sezer, O.; Siegel, D.; Bladé, J.; LeBlanc, R.; Sutherland, H.; Sopala, M.; Mishra, K. K.; *et al.* Phase Ib Study of Panobinostat and Bortezomib in Relapsed or Relapsed and Refractory Multiple Myeloma. *J. Clin. Oncol.* **2013**, *31*, 3696–3703.